Journal of Theoretical Medicine, 2002 Vol. 4 (4), pp. 251–270

Taylor & Francis
healthsciences

A Mathematical Model of an *In Vitro* Experiment to Investigate Endothelial Cell Migration

M.J. PLANK[a,*], B.D. SLEEMAN[a,†] and P.F. JONES[b]

[a]*School of Mathematics University of Leeds, Leeds LS2 9JT, UK;* [b]*Molecular Medicine Unit St. James' University Hospital, Leeds LS9 7TF, UK*

(Received 10 October 2002; In final form 10 June 2003)

Angiogenesis, the growth of new blood vessels from existing ones, is an important, yet not fully understood, process and is involved in diseases such as rheumatoid arthritis, diabetic retinopathy and solid tumour growth. Central to the process of angiogenesis are endothelial cells (EC), which line all blood vessels, and are capable of forming new capillaries by migration, proliferation and lumen formation. We construct a cell-based mathematical model of an experiment (Vernon, R.B. and Sage, E.H. (1999) "A novel, quantitative model for study of endothelial cell migration and sprout formation within three-dimensional collagen matrices", *Microvasc. Res.* **57**, 118–133) carried out to assess the response of EC to various diffusible angiogenic factors, which is a crucial part of angiogenesis. The model for cell movement is based on the theory of reinforced random walks and includes both chemotaxis and chemokinesis. Three-dimensional simulations are run and the results correlate well with the experimental data. The experiment cannot easily distinguish between chemotactic and chemokinetic effects of the angiogenic factors. We, therefore, also run two-dimensional simulations of a hypothetical experiment, with a point source of angiogenic factor. This enables directed (gradient-driven) EC migration to be investigated independently of undirected (diffusion-driven) migration.

Keywords: Angiogenesis; Collagen; Haptotaxis; Reinforced random walk; Chemotaxis

INTRODUCTION

Most primary solid tumours initiate as avascular clusters of cells (Folkman, 1974). Such a tumour must obtain the nutrients it needs by diffusion from a nearby capillary. The amount of nutrient that can be obtained in this way is limited and does not allow the tumour to grow beyond a certain size (typically about 1–2 mm in diameter) (Folkman, 1971). At this limiting size, the tumour is in a steady state, with cell proliferation balanced by cell death, and it may persist in this dormant phase for months or even years, without causing significant damage to the host (Carmeliet and Jain, 2000).

In order to grow further and to form metastases in distant organs, the tumour must obtain a blood supply. In many cases, this occurs by angiogenesis, the formation of new blood vessels from the existing vasculature (Paweletz and Kneirim, 1989). Angiogenesis takes place physiologically during embryogenesis (Risau, 1997), during placental growth and in the female reproductive system (Reynolds *et al.*, 1992). Angiogenesis can also be induced under pathological conditions, such as wound healing (Hunt *et al.*, 1984), rheumatoid arthritis (Carmeliet and Jain, 2000) and solid tumour growth (Folkman, 1971).

In the case of many solid tumours, angiogenesis never really stops. The tumour vasculature is constantly being remodelled, regressing in some areas and spreading in others (Vajkoczy *et al.*, 2002). If metastases form, angiogenesis will be induced at remote sites and the rapid malignant growth it permits will, unless the cancer is successfully treated, ultimately prove fatal.

Central to the process of angiogenesis are the endothelial cells (EC) which line all blood vessels in the body. In mature, quiescent capillaries, the EC form a single layer of flattened cells around the lumen. Cell–cell connections are tight and cell proliferation is rare (Han and Liu, 1999). The endothelium is surrounded by the basement membrane, an extra-cellular layer which serves as a scaffold on which the EC rest (Paweletz and Kneirim, 1989). Peri-endothelial support cells, such as smooth muscle cells and pericytes, are also found close to the capillary.

Tumours are known to secrete various chemicals, which diffuse into the surrounding tissue, some of which are

*Supported by EPSRC studentship number 00801007.
†Corresponding author. E-mail: bds@maths.leeds.ac.uk

ISSN 1027-3662 print/ISSN 1607-8578 online © 2002 Taylor & Francis Ltd
DOI: 10.1080/1027366031000159420

angiogenic growth factors (Folkman and Klagsbrun, 1987). The best characterised angiogenic factor is vascular endothelial growth factor (VEGF) (Yancopoulos *et al.*, 2000), which is largely specific for EC (Shweiki *et al.*, 1992) and has been shown to be a potent chemoattractant and mitogen (Klagsbrun and D'Amore, 1996; Han and Liu, 1999). During the dormant phase, the effects of these chemicals are outweighed by growth inhibitors, some of which may be present under normal physiological conditions, some of which may be produced by the immune system in response to the tumour, and some of which may be secreted by the tumour itself (Pepper, 1997; Carmeliet and Jain, 2000). However, at some point in time, the growth factors secreted by the tumour may finally overcome the inhibitors, and an angiogenic response is induced in the host (Hanahan and Folkman, 1996). The switch that triggers this emergence from dormancy into activity is still the subject for research, see for example Semenza (2000) and Giordano and Johnson (2001). Many factors are involved and hypoxia (oxygen deficiency), which is known to upregulate VEGF production (Shweiki *et al.*, 1992), is thought to have a major influence.

On receiving a VEGF stimulus, EC in capillaries near the tumour begin to loosen contacts with adjacent cells and secrete proteolytic enzymes, which degrade the basement membrane (Pepper, 1997). EC subsequently move through the gap in the basement membrane and into the extra-cellular matrix (ECM). They continue to secrete proteolytic enzymes, which also degrade the ECM (Pepper *et al.*, 1990). This allows them to migrate towards the tumour (Ausprunk and Folkman, 1977), thus forming sprouts from the parent capillary (Liotta *et al.*, 1991). The migration is thought to be controlled by chemotaxis (directed cell movement up a gradient of a diffusible substance, typically a growth factor emitted by the tumour) and haptotaxis (movement along an adhesive gradient, of fibronectin for example) (Carter, 1965).

In normal endothelia, the turnover for EC is very slow, typically measured in months or years (Han and Liu, 1999). Nevertheless, a short distance behind the sprout tips, rapid EC proliferation in response to VEGF is observed, increasing the rate of sprout formation (Ausprunk and Folkman, 1977; Denekamp and Hobson, 1982).

Sprouts are seen to branch and loop (anastomose) and the beginnings of a new vascular network are created, which gradually extends towards the tumour (Folkman and Klagsbrun, 1987). This branching and looping may become much more pronounced in the vicinity of the tumour, producing what is termed the brush-border effect (Muthukkaruppan *et al.*, 1982). Sprouts may eventually penetrate the tumour, providing it with the nutrients it needs for rapid growth. Once the tumour has established a blood supply, metastatic tumour cells can more easily enter the circulation and hence gain access to distant sites (Schirrmacher, 1985).

The sprouts do not form mature, stable capillaries with a continuous basement membrane and normal blood supply. Rather the new vasculature is irregular, leaky and tortuous (Hashizume *et al.*, 2000) and is constantly being remodelled as some sprouts regress and some vessels produce new sprouts (Vajkoczy *et al.*, 2002).

Understanding the response of EC to the many angiogenic and anti-angiogenic factors is of crucial importance in understanding the mechanisms by which solid tumours recruit new blood vessels, and hence in the search for effective anti-angiogenic therapeutic strategies. There has been increasing activity in recent years in constructing mathematical models of the process of angiogenesis. Much has been learned from this work about the complex process of angiogenesis, and it is the continuing aim of research in this field to further develop our understanding of the biological issues involved and to highlight potential therapeutic approaches.

The research can be divided broadly into two categories: continuous models at the cell density level; and discrete models at the level of the individual cell. Models of the continuous type are usually derived from mass conservation equations and chemical kinetics, or from continuum limit equations of random walks. This results in a system of partial differential equations (PDEs), modelling macroscopic quantities such as cell density and chemical concentrations. Examples include Balding and McElwain (1985), Chaplain and Stuart (1993), Chaplain *et al.* (1995) and Levine *et al.* (2001)

Discrete models, on the other hand, often contain a stochastic element and model at the level of the individual cell. They attempt to capture microscopic properties of the capillary network, such as sprout branching and looping, by keeping track of the movements of each individual cell. There are several different types of discrete model: for example, Stokes and Lauffenburger (1991) used stochastic differential equations to model the velocities of EC; Anderson and Chaplain (1998) derived an individual cell-based model by discretisation of a continuous system. The model presented here differs from these in that it attempts to link the continuous and discrete modelling approaches via the theory of reinforced random walks. This theory was developed by Davis (1990) and first applied in a biological context by Othmer and Stevens (1997). The technique has since been developed by Levine *et al.* (2001), Sleeman and Wallis (2002) and Plank and Sleeman (2003) and we believe it is an ideal framework for understanding the link between macroscopic and microscopic models.

Vernon and Sage (1999) carried out an *in vitro* experiment to study the response of EC to various angiogenic growth factors. In this article, we formulate a three-dimensional mathematical model of the experiment and run simulations for comparison with the experimental results. We also construct a simplified two-dimensional model of a hypothetical experiment, which isolates the *directional* response of the EC. The object of this work is to develop the modelling approach outlined above in close

conjunction with empirical data. We then aim to model a realistic *in vivo* scenario of tumour angiogenesis.

In the second section, the experimental setup is described in detail. In the third section, we build the mathematical model, which describes how the EC move and how the VEGF and collagen concentrations evolve. In the fourth section, the method of simulation is described. Finally, in the fifth section, the results are presented, discussed and compared with the experimental data.

THE EXPERIMENT

The experiment of Vernon and Sage (1999) investigates "radial invasion of matrix by aggregated cells" (RIMAC) in the presence of different growth factors. The assay consists of placing an aggregate of EC at the centre of a disc of collagen, immersed in medium $+/-$ angiogenic growth factors. After five days, the EC are scored for radial invasion into the surrounding collagen gel. See Fig. 1 for a diagram of the experimental setup. The growth factors tested, at varying levels and combinations, include VEGF, basic fibroblast growth factor (bFGF) and transforming growth factor-β1 (TGF-β1). Here, we concentrate on VEGF, the best characterised EC-specific growth factor (Han and Liu, 1999).

This is an experimental technique for assessing the response of cells to diffusing proteins in general. The aim of the experiment is to identify the effects of different angiogenic substances on EC migration. Clearly a thorough knowledge of the response of EC to the many chemicals involved is essential in understanding, and hopefully preventing, the angiogenic process.

Here we formulate this experiment as a reinforced random walk type model, which forms the basis for stochastic simulations of the experiment. The aim is to develop a modelling approach, which, while being mathematically tractable, is directly derived from the underlying biology. We believe this method has great potential to qualitatively model, among other things, the process of angiogenesis *in vivo*. Making comparisons between the predictions of the model and the results of the experiment may also help gauge realistic values for biological parameters, which is always a difficult part of mathematical modelling.

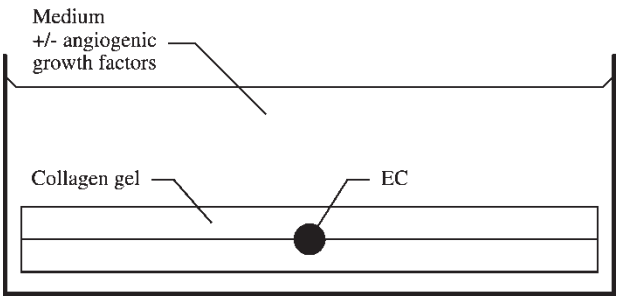

FIGURE 1 Diagram of the experiment.

In the full three-dimensional model, we assume that the VEGF concentration is in steady state. However, we also formulate a two-dimensional model in which we relax this assumption and allow for diffusion and uptake of VEGF. We then consider the effect of placing a point source of VEGF on the edge of the disc, in order to investigate the directional response of the EC to a chemotactic gradient (see Fig. 2).

THE MODEL

The model is constructed on a cylinder of radius R and height $2H$,

$$\Omega = \left\{(x, y, z) \in \mathbb{R}^3 : x^2 + y^2 \leq R^2, \quad -H \leq z \leq H\right\}.$$

Initially, collagen is distributed uniformly over the domain, representing the collagen gel. We neglect collagen diffusion since the rate of diffusion of large macromolecules such as collagen is very slow. EC are known to synthesise ECM components during sprout formation (Clark *et al.*, 1982; Jackson *et al.*, 1992) and so we include deposition of collagen by EC.

VEGF is applied at a constant concentration on the boundary, and is then allowed to diffuse throughout the domain. A term is included modelling uptake and binding of VEGF by the EC. Upper and lower functions for the solution to the resulting reaction-diffusion equation for VEGF are obtained using comparison principles. Simulations are then run with the steady state solutions of both the upper and the lower functions.

The EC are initially arranged in a spherical aggregate (of radius $r_i < H < R$) at the centre of the domain. Each cell is subsequently permitted to move around on a regular finite grid, obeying the rules of a reinforced random walk (Davis, 1990). VEGF is viewed as a chemotactic and chemokinetic factor for EC (Klagsbrun and D'Amore, 1996; Han and Liu, 1999). In other words, VEGF promotes both random

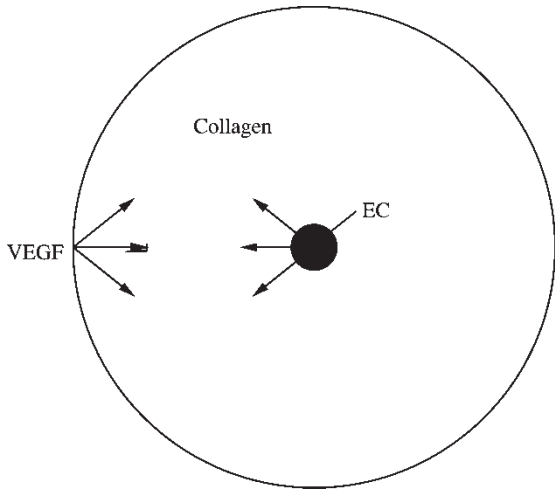

FIGURE 2 Two-dimensional model with a point source of VEGF.

migration and directed migration up a VEGF concentration gradient. Collagen is assumed to assist EC adhesion by haptotaxis (Bowersox and Sorgente, 1982; Anderson and Chaplain, 1998; Holmes and Sleeman, 2000). The random walk is therefore set up so that EC are attracted to areas of higher VEGF and higher collagen concentrations. The behaviour of the EC is then examined under various conditions, and the results compared to the experimental results seen by Vernon and Sage (1999).

Thus the three quantities of interest are the EC density, $p(x, y, z, t)$, the VEGF concentration, $v(x, y, z, t)$, and the collagen concentration, $c(x, y, z, t)$ at (x, y, z) and time t.

The Endothelial Cell Dynamics

For clarity, the equations in this section will be presented in two dimensions, but readily generalise to the three-dimensional form used in the simulations. We assume that the EC move on a regular grid (of step size h) and denote the EC (probability) density at grid point (n,m) at time t by $p_{n,m}(t)$.

Othmer and Stevens (1997) used the reinforced random walk master equation to simulate cell movement on a regular lattice:

$$\begin{aligned}\frac{\partial p_{n,m}}{\partial t} &= \hat{\tau}^{\mathrm{H}+}_{n-1,m}\,p_{n-1,m} + \hat{\tau}^{\mathrm{H}-}_{n+1,m}\,p_{n+1,m} \\ &\quad + \hat{\tau}^{\mathrm{V}+}_{n,m-1}p_{n,m-1} + \hat{\tau}^{\mathrm{V}-}_{n,m+1}p_{n,m+1} \\ &\quad - \left(\hat{\tau}^{\mathrm{H}+}_{n,m} + \hat{\tau}^{\mathrm{H}-}_{n,m} + \hat{\tau}^{\mathrm{V}+}_{n,m} + \hat{\tau}^{\mathrm{V}-}_{n,m}\right)p_{n,m}, \qquad (1)\end{aligned}$$

where $\hat{\tau}^{\mathrm{H}\pm}_{n,m}$ and $\hat{\tau}^{\mathrm{V}\pm}_{n,m}$ are the transition rates of EC moving from (n, m) to $(n \pm 1, m)$ and $(n, m \pm 1)$ respectively[‡]. Note that these transition rates may depend on one or more control substances; in our case, the control substances are VEGF and collagen.

Othmer and Stevens (1997) made the assumption that the decision "when to move" is independent of the decision "where to move":

$$\hat{\tau}^{\mathrm{H}+}_{n,m} + \hat{\tau}^{\mathrm{H}-}_{n,m} + \hat{\tau}^{\mathrm{V}+}_{n,m} + \hat{\tau}^{\mathrm{V}-}_{n,m} = 4\lambda \qquad (2)$$

for $\lambda > 0$ constant. Hence the mean waiting time at a grid point is constant, $(1/(4\,\lambda))$, and the control substances only affect the direction of movement, not the rate of movement.

They further assumed that the transition probabilities depend only on the control substances at the nearest 1/2 neighbour grid points, and took

$$\hat{\tau}^{\mathrm{H}\pm}_{n,m} = \frac{4\lambda\tau\left(w_{n\pm\frac{1}{2},m}\right)}{\tau\left(w_{n-\frac{1}{2},m}\right)+\tau\left(w_{n+\frac{1}{2},m}\right)+\tau\left(w_{n,m-\frac{1}{2}}\right)+\tau\left(w_{n,m+\frac{1}{2}}\right)}, \qquad (3)$$

$$\hat{\tau}^{\mathrm{V}\pm}_{n,m} = \frac{4\lambda\tau\left(w_{n,m\pm\frac{1}{2}}\right)}{\tau\left(w_{n-\frac{1}{2},m}\right)+\tau\left(w_{n+\frac{1}{2},m}\right)+\tau\left(w_{n,m-\frac{1}{2}}\right)+\tau\left(w_{n,m+\frac{1}{2}}\right)}, \qquad (4)$$

for some function, $\tau(w)$, where $w=(v,c)$, the vector of control substances.

Under this choice, it can be shown (Othmer and Stevens, 1997) that the continuum limit, $h \to 0$, $\lambda \to \infty$, such that $\lambda h^2 = D$ of the master Eq. (1) is

$$\frac{\partial p}{\partial t} = D\nabla\cdot\left(p\nabla\left(\ln\frac{p}{\tau(v,c)}\right)\right).$$

This may be written in the more familiar form

$$\frac{\partial p}{\partial t} = D\nabla^2 p - \nabla\cdot(p(\chi(v)\nabla v + \rho(c)\nabla c)),$$

on making the choice

$$\begin{aligned}\tau(v,c) &= \tau_1(v)\tau_2(f) \\ &= \exp\left(\frac{1}{D}\int\chi(v)\mathrm{d}v\right)\exp\left(\frac{1}{D}\int\rho(c)\mathrm{d}c\right). \qquad (5)\end{aligned}$$

$\chi(v)$ and $\rho(f)$ are respectively the chemotactic and haptotactic sensitivities, and so the total flux, J, of EC consists of a Fickian diffusive component, a chemotactic component and a haptotactic component:

$$J = J_{\mathrm{diff}} + J_{\mathrm{chem}} + J_{\mathrm{hapt}} = -D\nabla p + \chi(v)p\nabla v + \rho(c)p\nabla c.$$

Notice how the transition probability function, τ, survives the process of taking the continuum limit of the master equation, thereby providing a natural link between discrete and continuous models. Sleeman and Wallis (2002) and Plank and Sleeman (2003) used the master equation (1) as the basis for simulations of EC movement in tumour angiogenesis. Here, we wish to include not only taxis (i.e. gradient-driven) effects, but also chemokinetic (i.e. random diffusive) effects of the control substances. In order to achieve this, we relax the assumption (2) of constant mean waiting times.

In addition to the normalised reinforced random walk model resulting from Eqs.(3) and (4), Othmer and Stevens (1997) considered an unnormalised model, in which the transition rates were chosen as follows.

$$\hat{\tau}^{\mathrm{H}\pm}_{n,m} = \lambda T\left(w_{n\pm\frac{1}{2},m}\right),$$

$$\hat{\tau}^{\mathrm{V}\pm}_{n,m} = \lambda T\left(w_{n,m\pm\frac{1}{2}}\right),$$

for some function $T(w)$.

[‡]The superscripts, H and V, denote jumps in the horizontal and vertical directions respectively.

The resulting continuum limit of Eq. (1) is

$$\frac{\partial p}{\partial t} = \nabla\cdot(T(w)\nabla p).$$

Hence there is no taxis, and the dynamics are driven purely by the random diffusive flux, $J = -T(w)\nabla p$. $T(w)$ may be thought of as the diffusion coefficient, D, which is no longer a constant, but now depends on the control substance, w.

We combine the normalised and unnormalised probabilities, to incorporate both chemotactic and chemokinetic effects, by choosing the transition rates as follows.

$$\hat{\tau}^{\mathrm{H}\pm}_{n,m} = \lambda\left(\frac{4\tau\left(w_{n\pm\frac{1}{2},m}\right)}{\tau\left(w_{n-\frac{1}{2},m}\right)+\tau\left(w_{n+\frac{1}{2},m}\right)+\tau\left(w_{n,m-\frac{1}{2}}\right)+\tau\left(w_{n,m+\frac{1}{2}}\right)} + \frac{D\left(w_{n\pm\frac{1}{2},m}\right)}{D_0} - 1\right), \tag{6}$$

$$\hat{\tau}^{\mathrm{V}\pm}_{n,m} = \lambda\left(\frac{4\tau\left(w_{n,m\pm\frac{1}{2}}\right)}{\tau\left(w_{n-\frac{1}{2},m}\right)+\tau\left(w_{n+\frac{1}{2},m}\right)+\tau\left(w_{n,m-\frac{1}{2}}\right)+\tau\left(w_{n,m+\frac{1}{2}}\right)} + \frac{D\left(w_{n,m\pm\frac{1}{2}}\right)}{D_0} - 1\right), \tag{7}$$

for some function $D(w)$ and constant $D_0 > 0$.

Now, the continuum limit $h \to 0$, $\lambda \to \infty$, such that $\lambda h^2 = D_0$ of the master equation (1) is

$$\frac{\partial p}{\partial t} = D_0\nabla\cdot\left(p\nabla\left(\ln\frac{p}{\tau(v,c)}\right)\right) + \nabla\cdot((D(v,c)-D_0)\nabla p) \tag{8}$$

$$= \nabla\cdot\left(D(v,c)\nabla p - D_0 p\frac{\nabla\tau(v,c)}{\tau(v,c)}\right). \tag{9}$$

Making the same choice for the transition probability function (5) (with D replaced by D_0), we may again write this in a more familiar form:

$$\frac{\partial p}{\partial t} = \nabla\cdot(D(v,c)\nabla p) - \nabla\cdot(p(\chi(v)\nabla v + \rho(c)\nabla c)). \tag{10}$$

To summarise, the addition of an unnormalised component in the transition rates results in a variable diffusion coefficient in the continuum limit PDE (10), which we are free to choose. This is unsurprising given the fact that unnormalised transition rates are associated with a purely diffusive continuum limit, without any taxis terms. The one disadvantage of this method is the introduction of the arbitrary parameter, $D_0 > 0$, in the transition rates, to which the continuum limit PDE is invariant.

Note that the same goal (i.e. the appearance of a variable diffusion coefficient in the continuum limit) may also be achieved by using the original, normalised form of the transition probabilities (3) and (4), but allowing the waiting time parameter, λ, to depend on the control substance values at the barrier to be crossed:

$$\hat{\tau}^{\mathrm{H}\pm}_{n,m} = \frac{4\lambda\left(w_{n\pm\frac{1}{2},m}\right)\tau\left(w_{n\pm\frac{1}{2},m}\right)}{\tau\left(w_{n-\frac{1}{2},m}\right)+\tau\left(w_{n+\frac{1}{2},m}\right)+\tau\left(w_{n,m-\frac{1}{2}}\right)+\tau\left(w_{n,m+\frac{1}{2}}\right)},$$

$$\hat{\tau}^{\mathrm{V}\pm}_{n,m} = \frac{4\lambda\left(w_{n,m\pm\frac{1}{2}}\right)\tau\left(w_{n,m\pm\frac{1}{2}}\right)}{\tau\left(w_{n-\frac{1}{2},m}\right)+\tau\left(w_{n+\frac{1}{2},m}\right)+\tau\left(w_{n,m-\frac{1}{2}}\right)+\tau\left(w_{n,m+\frac{1}{2}}\right)}.$$

The problem with this approach is that, in the case where there is more than one control substance and more than one spatial dimension, there is no well defined function, τ, for which the continuum limit PDE is equivalent to Eq. (10). We therefore adopt the transition probabilities (6), (7) and choose D_0 to be the minimum value of $D(w)$ (to ensure that $D(w) - D_0 \geq 0$)[¶].

Various choices are possible for the sensitivities, $\chi(v)$ and $\rho(c)$. The simplest is to take constant values, $\chi(v) = \chi_0$, $\rho(c) = \rho_0$, leading to classical chemotaxis and haptotaxis (Keller and Segel, 1971; Murray, 1993). We make the more realistic assumption that EC sensitivity is reduced in regions where the concentration of chemoattractant is high, reflecting desensitisation of the cell receptors. Following Balding and McElwain (1985) and Anderson and Chaplain (1998), we therefore take a receptor-kinetic law of the form

$$\chi(v) = \frac{\chi_0}{1+\gamma_1 v}. \tag{11}$$

In the absence of evidence regarding functional forms, we assume that the response to collagen (that is, haptotaxis) occurs by the same mechanism as chemotaxis. We therefore take $\tau(v,c) = \tau_1(v)\tau_2(c)$ where

$$\tau_1(v) = (1+\gamma_1 v)^{\frac{\chi_0}{\gamma_1 D_0}}, \tag{12}$$

$$\tau_2(c) = (1+\gamma_2 c)^{\frac{\rho_0}{\gamma_2 D_0}}, \tag{13}$$

and $\chi_0, \rho_0, \gamma_1, \gamma_2$ are constants.

Since the EC are stimulated to move up VEGF gradients and up collagen gradients, we take $\chi_0, \rho_0 > 0$. So that the desensitisation of cell receptors occurs at biologically realistic levels of v and c, we choose γ_1 to be of order $O(v^{-1})$ and γ_2 to be $O(c^{-1})$.

In addition to the directional response of the EC to VEGF and collagen, we wish to model an increase in random motility at higher VEGF concentrations. We wish $D(w)$ to be an increasing function of v, which varies

[¶]The effects of changing D_0 will be discussed in the "Results and Discussion" section.

between positive upper and lower bounds. We therefore take the rational form

$$D(v) = D_m \frac{v+\theta_1}{v+\theta_2}. \tag{14}$$

for constants $D_m > 0$ and $0 < \theta_1 < \theta_2$. $D(0) = D_m \frac{\theta_1}{\theta_2}$ and so there will still be some random motility in the absence of any VEGF. $D(v) \to D_m$ as $v \to \infty$ and so the diffusion coefficient does not increase without bound as the VEGF concentration grows very large, but saturates to a limiting value.

Initially, there is an aggregate of EC (of radius r_i) centred on (0,0,0) and no cells elsewhere. We therefore start by positioning one EC at each grid point in $\{(x,y,z) \in \Omega : x^2+y^2+z^2 \le r_i^2\}$. The EC cannot move outside the disc and so we impose no flux of EC across the boundary $\partial\Omega$.

These conditions may be written (in continuum form) as

$$p(x,y,z,0) = \begin{Bmatrix} p_0 & x^2+y^2+z^2 \le r_i^2 \\ 0 & x^2+y^2+z^2 > r_i^2 \end{Bmatrix}, \tag{15}$$

$$0 = D(v)\frac{\partial p}{\partial n} - D_0 \frac{p}{\tau}\frac{\partial \tau}{\partial n}, \quad \text{on } \partial\Omega \times [0,T], \tag{16}$$

where $\frac{\partial}{\partial n}$ is the normal derivative on the boundary $\partial\Omega$.

The continuum equations given in this subsection are included to demonstrate the technique of relating the reinforced random walk master equation to a continuum limit PDE, *and are not solved numerically in the simulations*. Instead we use the master equation (1), with transition probabilities given by Eqs. (6), (7), (12)–(14), to simulate EC movement on a regular grid (see "Method of Simulation" section).

The VEGF and Collagen Dynamics

VEGF binds to receptors on the endothelial cell surface and this stimulates the EC to produce a proteolytic enzyme (or protease), capable of degrading extra-cellular proteins (Pepper, 1997). Here, we are not concerned with proteolysis, but we do incorporate uptake of VEGF by EC, which we assume occurs at constant rate, $\alpha \ge 0$. We include a natural, Fickian diffusion term (with diffusion coefficient, D_v) to arrive at the governing equation for VEGF:

$$\frac{\partial v}{\partial t} = D_v \nabla^2 v - \alpha p v, \quad \text{on } \Omega \times [0,T]. \tag{17}$$

In the experiment (Vernon and Sage, 1999), there is initially no VEGF in the domain, except on the boundary where it is at a uniform level, $v_0 > 0$. This gives the initial condition

$$v(x,y,z,0) = \begin{Bmatrix} 0 & \text{inside } \Omega \\ v_0 & \text{on } \partial\Omega \end{Bmatrix}. \tag{18}$$

Furthermore, since the disc is suspended in a relatively large container of medium, the VEGF concentration on the boundary can be assumed to remain at this constant level throughout. We therefore have the Dirichlet boundary condition,

$$v(x,y,z,t) = v_0, \quad \text{on } \partial\Omega \times [0,T]. \tag{19}$$

In the experiment, the disc was initially covered with a collagen gel of uniform concentration. In addition to this initial level, we model the EC as laying down collagen (Paweletz and Kneirim, 1989; Jackson *et al.*, 1992), according to the logistic growth equation used by Levine *et al.* (2001):

$$\frac{\partial c}{\partial t} = \beta p c (C - c), \quad \text{on } \Omega \times [0,T], \tag{20}$$

where β,$C \ge 0$ are constants.

Thus the collagen concentration will increase in the presence of EC (when $p > 0$), but cannot rise above a fixed maximum concentration, C. Collagen is a large macromolecule and so its diffusion will take place very slowly. We therefore neglect collagen diffusion.

The collagen is initially of uniform concentration, $c_0 \in (0, C)$, giving the initial condition

$$c(x,y,z,0) = c_0, \quad \text{on } \Omega. \tag{21}$$

Non-dimensionalisation

We non-dimensionalise by setting

$$p' = \tfrac{p}{p_0}, \quad v' = \tfrac{v}{V}, \quad c' = \tfrac{c}{C}, \quad x' = \tfrac{x}{R}, \quad y' = \tfrac{y}{R}, \quad z' = \tfrac{z}{R}$$
$$t' = \tfrac{t}{T}, \quad D_m{}' = \tfrac{D_m T}{R^2}, \quad D_0{}' = \tfrac{D_0 T}{R^2}, \quad D_v{}' = \tfrac{D_v T}{R^2}, \quad \alpha' = Tp_0\alpha, \quad \beta' = Tp_0 C\beta$$
$$\gamma_1{}' = V\gamma_1, \quad \gamma_2{}' = C\gamma_2, \quad v_0{}' = \tfrac{v_0}{V}, \quad c_0{}' = \tfrac{c_0}{C}, \quad \theta_1{}' = \tfrac{\theta_1}{V}, \quad \theta_2{}' = \tfrac{\theta_2}{V}$$
$$H' = \tfrac{H}{R}, \quad q_1 = \tfrac{\chi_0}{\gamma_1 D_0}, \quad q_2 = \tfrac{\rho_0}{\gamma_2 D_0}, \quad r_i{}' = \tfrac{r_i}{R}.$$

The governing Eqs. (1), (17) and (20), on dropping the dashes, become

$$\frac{\partial p_{n,m}}{\partial t} = \hat{\tau}^{\mathrm{H}+}_{n-1,m} p_{n-1,m} + \hat{\tau}^{\mathrm{H}-}_{n+1,m} p_{n+1,m} + \hat{\tau}^{\mathrm{V}+}_{n,m-1} p_{n,m-1} + \hat{\tau}^{\mathrm{V}-}_{n,m+1} p_{n,m+1} - (\hat{\tau}^{\mathrm{H}+}_{n,m} + \hat{\tau}^{\mathrm{H}-}_{n,m} + \hat{\tau}^{\mathrm{V}+}_{n,m} + \hat{\tau}^{\mathrm{V}-}_{n,m}) p_{n,m}, \tag{22}$$

$$\frac{\partial v}{\partial t} = D_v \nabla^2 v - \alpha p v, \tag{23}$$

$$\frac{\partial c}{\partial t} = \beta p c (1 - c), \tag{24}$$

on $\Omega = \{(x,y,z) \in \mathbb{R}^3 : x^2+y^2 \le 1, -H \le z \le H\}$, $t \in [0,1]$.

The transition rates (6), (7), (12)–(14) are given by

$$\hat{\tau}^{\mathrm{H}\pm}_{n,m} = \lambda\left(\frac{4\tau(w_{n\pm\frac{1}{2},m})}{\tau(w_{n-\frac{1}{2},m})+\tau(w_{n+\frac{1}{2},m})+\tau(w_{n,m-\frac{1}{2}})+\tau(w_{n,m+\frac{1}{2}})} + \frac{D(w_{n\pm\frac{1}{2},m})}{D_0} - 1\right), \tag{25}$$

$$\hat{\tau}^{\mathrm{V}\pm}_{n,m} = \lambda\left(\frac{4\tau(w_{n,m\pm\frac{1}{2}})}{\tau(w_{n-\frac{1}{2},m})+\tau(w_{n+\frac{1}{2},m})+\tau(w_{n,m-\frac{1}{2}})+\tau(w_{n,m+\frac{1}{2}})} + \frac{D(w_{n,m\pm\frac{1}{2}})}{D_0} - 1\right), \tag{26}$$

where

$$\tau(v,c) = (1+\gamma_1 v)^{q_1}(1+\gamma_2 c)^{q_2}, \tag{27}$$

$$D(v) = D_m\frac{v+\theta_1}{v+\theta_2}, \tag{28}$$

$$\lambda = \frac{D_0}{h^2}. \tag{29}$$

The initial conditions (15), (18), (21) and boundary conditions (16), (19) become

$$\text{On } \Omega: \quad p(x,y,z,0) = \left\{\begin{array}{ll} 1 & x^2+y^2+z^2 \le r_i^2 \\ 0 & x^2+y^2+z^2 > r_i^2 \end{array}\right\},$$

$$\text{On } \partial\Omega\times[0,1]: \quad \frac{D(v)}{D_0 p}\frac{\partial p}{\partial n} = \frac{1}{\tau}\frac{\partial \tau}{\partial n}, \tag{30}$$

$$\text{On } \Omega: \quad v(x,y,z,0) = \left\{\begin{array}{ll} 0 & \text{inside } \Omega \\ v_0 & \text{on } \partial\Omega \end{array}\right\},$$

$$\text{On } \partial\Omega\times[0,1]: \quad v(x,y,z,t) = v_0, \tag{31}$$

$$\text{On } \Omega: \quad c(x,y,z,0) = c_0. \tag{32}$$

In the three-dimensional simulations, we do not wish to solve the full reaction-diffusion equation for VEGF (23). We therefore construct lower and upper functions (v_1 and v_2 respectively) for the solution to this equation using comparison principles (see appendix A for details). The solution, v, of Eq. (23) thus satisfies

$$v_1(x,y,z,t) \le v(x,y,z,t) \le v_2(x,y,z,t) \quad \text{on } \Omega\times[0,1].$$

In the case of the lower function, v_1, the solution rapidly evolves to a steady state, $v_{1,s}$. For the upper function, v_2, evolution to the steady state, $v_{2,s}$ (which is spatially homogeneous), takes place more slowly. Nevertheless, $v_{2,s}$ is still an upper function for v and so we will use the steady states $v_{1,s}$ and $v_{2,s}$ in the simulations. The effects of using the time-dependent upper solution, which is intermediate between these two extremes and is likely to approximate the actual VEGF profile more closely, will also be discussed. The steady state solutions are given by:

$$v_{1,s}(x,y,z) = v_0\left(\frac{\cosh\left(\sqrt{\frac{\alpha}{D_v}}z\right)}{\cosh\left(\sqrt{\frac{\alpha}{D_v}}H\right)} + \sum_{n=1}^{\infty} A_n I_0\left(\sqrt{\lambda_n}r\right)\cos\left((2n-1)\frac{\pi z}{2H}\right)\right), \tag{33}$$

$$v_{2,s}(x,y,z) = v_0, \tag{34}$$

where

$$\lambda_n = \frac{\alpha}{D_v} + \frac{\pi^2(2n-1)^2}{4H^2},$$

I_0 is the modified Bessel function of the first kind and zeroeth order, and the A_n are Fourier coefficients. One set of simulations is run with $v = v_{1,s}$ and one set with $v = v_{2,s}$.

We subsequently run two-dimensional simulations, on $\bar{\Omega} = \{(x,y) \in \mathbb{R}^2 : x^2+y^2 \le 1\}$ with the full VEGF dynamics (23). However, in order to isolate the directional response of the EC, we modify the initial and boundary conditions for VEGF to represent a point source at $(x,y) = (-1,0)$, as opposed to a uniform source on $\partial\bar{\Omega}$. We therefore use the conditions

$$v(x,y,z,0) = \left\{\begin{array}{ll} 0 & \text{inside } \bar{\Omega} \\ v_0\exp(-K((x+1)^2+y^2)) & \text{on } \partial\bar{\Omega} \end{array}\right\}, \tag{35}$$

$$v(x,y,z,t) = v_0\exp\left(-K((x+1)^2+y^2)\right) \text{ on } \partial\bar{\Omega}\times[0,1]. \tag{36}$$

METHOD OF SIMULATION

The time span [0,1] is divided into time steps of length k. The EC move on a regular grid of step size h. The control substances are calculated on a half-step grid, such that between any two adjacent cell grid points, there is exactly one control substance grid point.

The method of simulation of cell movement is based on that of Sleeman and Wallis (2002) as follows. At each time step, the movement of each EC is simulated in turn, according the master equation (22). The probabilities of that particular cell staying still, moving one step to the left, right, up and down are calculated according to Eqs. (25) and (26). These probabilities depend on the nearest $\frac{1}{2}$ neighbour levels of VEGF and collagen via the transition probability function (27) and the diffusion coefficient (28). The real interval [0,1] is divided into five sub-intervals (one for staying still, one for moving left and so on)

each of length equal to the relevant probability. A random number $r \in [0,1)$ is then generated and, depending on the sub-interval in which this number falls, the cell stays still or moves in the appropriate direction (unless the direction it wants to move in is blocked by another cell, in which case it stays still):

$$\text{Move left if} \quad r \in \left[0, \hat{\tau}^{\mathrm{H}-}_{n,m} k\right).$$

$$\text{Move right if} \quad r \in \left[\hat{\tau}^{\mathrm{H}-}_{n,m} k, \hat{\tau}^{\mathrm{H}-}_{n,m} k + \hat{\tau}^{\mathrm{H}+}_{n,m} k\right).$$

$$\text{Move down if} \quad r \in \left[\hat{\tau}^{\mathrm{H}-}_{n,m} k + \hat{\tau}^{\mathrm{H}+}_{n,m} k, \hat{\tau}^{\mathrm{H}-}_{n,m} k + \hat{\tau}^{\mathrm{H}+}_{n,m} k + \hat{\tau}^{\mathrm{V}-}_{n,m} k\right).$$

$$\text{Move up if} \quad r \in \left[\hat{\tau}^{\mathrm{H}-}_{n,m} k + \hat{\tau}^{\mathrm{H}+}_{n,m} k + \hat{\tau}^{\mathrm{V}-}_{n,m} k, \hat{\tau}^{\mathrm{H}-}_{n,m} k + \hat{\tau}^{\mathrm{H}+}_{n,m} k + \hat{\tau}^{\mathrm{V}-}_{n,m} k + \hat{\tau}^{\mathrm{V}+}_{n,m} k\right).$$

$$\text{Stay still if} \quad r \in \left[\hat{\tau}^{\mathrm{H}-}_{n,m} k + \hat{\tau}^{\mathrm{H}+}_{n,m} k + \hat{\tau}^{\mathrm{V}-}_{n,m} k + \hat{\tau}^{\mathrm{V}+}_{n,m} k, 1\right).$$

The method of simulation has, for clarity, been described in two dimensions, but the three-dimensional simulations are carried out in the same way, defining a third set of transition rates, for movement in the z-direction, analogously to Eqs. (25) and (26). Note that if a cell ever reaches a mesh point adjacent to the boundary of the domain, it plays no further part in the simulation.

In the two-dimensional simulations, the VEGF values are updated at each time step according to Eq. (23), using a Crank-Nicholson numerical method.

The equation for collagen (24) may be solved to give

$$c(x,y,z,t+k) = \left[1 + \left(\frac{1}{c(x,y,z,t)} - 1\right)\exp\left(-\beta \int_t^{t+k} p(x,y,z,s)\,\mathrm{d}s\right)\right]^{-1},$$

which is used to update the collagen values at each time step.

Note that the control substances are computed on an embedded lattice that is twice as fine as the lattice for cell movement. When updating values at a control substance node that is also on the cell movement lattice, $p(x,y,z,t)$ is taken to be 1 if the point (x,y,z) is occupied at time t and 0 if it is empty. At nodes that are not on the cell movement lattice, $p(x,y,z,t)$ is taken to be an average of the values at the adjacent points on the cell movement lattice.

At the end of the simulation, the cells are scored for radial invasion in the same way as in the Vernon and Sage (1999) experiment. That is, the disc is divided into 64 equal segments and the maximum radial invasion distance (regardless of the distance travelled in the z-direction) in each segment is noted. The average of these 64 values is then used as the radial invasion number.

The parameter values used in the simulations are, unless otherwise stated, as shown in Table I (see appendix B for a discussion of these values).

TABLE I Parameter values used in the simulations

Dimensional values	
Length of time of experiment	$T = 120\ h$
Radius of disc	$R = 1.4\,\mathrm{mm}$
Half-height of disc	$R = 0.7\,\mathrm{mm}$
Radius of EC aggregate	$r_i = 0.134\,\mathrm{mm}$
Maximum EC diffusion coefficient	$D_m = 3.6 \times 10^{-4}\,\mathrm{mm}^2/h$
EC diffusion coefficient parameters	$\theta_1 = 2.5 \times 10^{-4}\ \mu g/\mathrm{ml}$
	$\theta_2 = 2.5 \times 10^{-3}\ \mu g/\mathrm{ml}$
VEGF diffusion coefficient	$D_v = 3.6 \times 10^{-3}\,\mathrm{mm}^2/h$
Chemotactic coefficient	$\chi_0 = 5.67\,\mathrm{mm}^2 h^{-1} ml\mu g^{-1}$
Haptotactic coefficient	$\rho_0 = 7.88 \times 10^{-7}\,\mathrm{mm}^2 h^{-1} ml\mu g^{-1}$
EC density in initial aggregate	$\rho_0 = 4444\,\mathrm{mm}^{-1}$
Boundary VEGF concentration	$V = v_0 = 5 \times 10^{-3} ml\mu/g$
Initial collagen concentration	$c_0 = 600\ \mu g/\mathrm{ml}$
Maximum collagen concentration	$C = 2400\ \mu g/\mathrm{ml}$
VEGF uptake rate	$\alpha = 8.66 \times 10^{-5}\,\mathrm{mm}^2/h$
Collagen production coefficient	$\beta = 1.72 \times 10^{-9}\,\mathrm{mm}^2/h^{-1} ml\mu g^{-1}$
Saturating parameter for VEGF	$\gamma = 2000\,\mathrm{ml}/\mu g$
Saturating parameter for collagen	$\gamma_2 = 8.34 \times 10^{-4}\,\mathrm{ml}/\mu g$
Grid size	$h = 1.50 \times 10^{-2}\,\mathrm{mm}$
Time step size	$k = 0.12\ h$
Dimensionless values	
Half-height of disc	$H = 0.5$
Maximum EC diffusion coefficient	$D_m = 0.0220$
EC diffusion coefficient parameters	$\theta_1 = 0.05$
	$\theta_2 = 0.5$
VEGF diffusion coefficient	$D_v = 0.220$
Exponent in VEGF transition probability function	$q_1 = (\chi_0/r_1 D_p) = 78.8$
Exponent in collagen transition probability function	$q_2 = (\rho_0/r_2 D_p) = 26.3$
Boundary VEGF concentration	$v_0 = 1$
Initial collagen concentration	$c_0 = 0.25$
VEGF uptake coefficient	$\alpha = 46.2$
Collagen production coefficient	$\beta = 46.2$
Radius of EC aggregate	$r_i = 9.59 \times 10^{-2}$
Saturation parameter for VEGF	$\gamma_1 = 10$
Saturation parameter for collagen	$\gamma_2 = 2$
Grid size	$h = 1.08 \times 10^{-2}$
Time step size	$k = 1 \times 10^{-3}$

RESULTS AND DISCUSSION

Simulations of the system (22), (24)–(32) were run in three dimensions, firstly with VEGF concentration given by Eq. (34), and secondly by Eq. (33). Various boundary values for the VEGF concentration, v_0, were used.

Figure 3 shows a graph of radial invasion (as defined in the "Method of Simulation" section) against v_0, the VEGF concentration on the edge of the disc, using the upper solution (34). As one would expect, increasing the VEGF level increases the invasive capacity of the cells; moreover, the graph exhibits good agreement with the experimental results shown in Fig. 4. Since the VEGF concentration (34) is spatially uniform, there is no chemotaxis (gradient-driven migration) and the stimulus is entirely chemokinetic (diffusion-driven migration).

Figure 5 shows a plan view of the EC (i.e. their positions in the xy-plane) at $t = 0.0$, $t = 0.2$, $t = 0.4$, $t = 0.6$, $t = 0.8$ and $t = 1.0$ in a simulation using the upper solution for VEGF (34) and $v_0 = 1$. As expected, the cells gradually invade the surrounding matrix over time. Comparing the final positions of the EC in Fig. 5 with

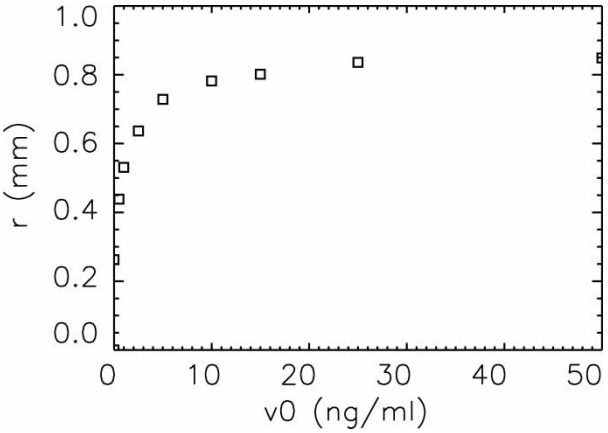

FIGURE 3 Average radial invasion against v_0, the VEGF concentration on the edge of this disc, using the upper solution for VEGF (34).

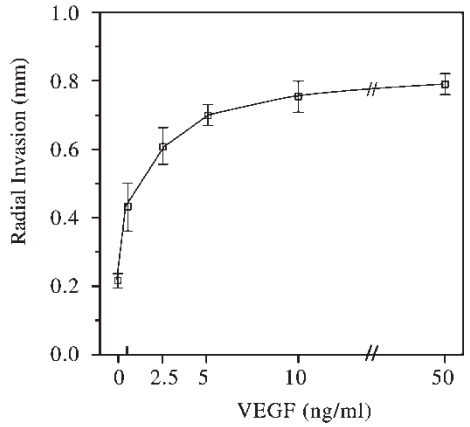

FIGURE 4 Experimental results of Vernon and Sage (1999): graph of radial invasion against boundary concentration of VEGF.

experimental results (Fig. 10(a)) shows that they are qualitatively similar: the cells form outward trails from the initial aggregate in response to chemokinetic effects of VEGF. Figure 6 shows the positions of the same cells in the xz-plane, illustrating the migration in the vertical (z) direction. Note that several cells have reached the upper and lower boundaries of the disc ($z = \pm 0.5$), from where they can move no further.

Figure 7 shows how the collagen profile develops; the concentration is plotted for $-H \leq z \leq H$ along the radial line $-1 \leq x \leq 1,\ y = 0$.[§] Since collagen diffusion is neglected in the model, the collagen level can only rise above its initial value where an EC is present. Unsurprisingly, it is in the centre of the domain, where the main body of cells is concentrated, that the collagen levels increase most rapidly. As time progresses, collagen is also laid down in areas away from the centre by invading cells. Although the profiles are rather erratic, it is clear that, at a given point in time, the general trend is for the collagen levels to decrease as one moves away from the centre. Thus, broadly speaking, haptotaxis will have the effect of holding the cells back.

It is possible that a number of cells are able to escape from the initial aggregate and subsequently move some distance into the matrix. As time passes, however, it becomes increasingly difficult to break away from the main cluster of cells due to the strong inward pull of haptotaxis.

Figure 8 show a simulation with $v_0 = 0.2$ (i.e. VEGF at one fifth of the standard concentration). Compared with Fig. 5, the radial distances travelled by the EC into the matrix are significantly less. This reduced invasive capacity is due to the reduced diffusion coefficient of the EC (28). Vernon and Sage (1999) observed similar results at half the standard VEGF concentration: Fig. 10(b) shows fewer invading cells and smaller invasion distances than Fig. 10(a).

Figure 9 shows a simulation with no VEGF. Very few EC manage to break away from the initial aggregate and these do not move very far into the matrix. Again, the corresponding result of Vernon and Sage (1999), Fig. 10(c), shows good agreement, with very few cells moving very small distances.

Figure 11 shows the results of a simulation using the *lower* solution for VEGF (33). The VEGF profile Fig. 11(c) is no longer spatially uniform, but decreases as one moves towards the centre of the disc. There is therefore now a chemotactic stimulus for the EC to move up the VEGF concentration gradient, towards the boundary of the disc, in addition to the chemokinetic effects. Somewhat surprisingly, the radial invasion distances are significantly less than in the spatially uniform case (see Fig. 5). However, the vertical migration distances are greater, with a large number of EC accumulating on the upper and lower surfaces of the disc. The reason for this is that the radius of the cylindrical domain, R, is greater than its height, H, and so the distance between the initial aggregate and the upper and lower boundaries is less than the distance to the outer boundary. The VEGF gradient is steeper nearer to the boundary, $\partial\Omega$, and so the EC are exposed to a greater chemotactic gradient in the z direction than in the x and y directions. Hence in this case chemotaxis favours vertical, as opposed to radial, migration.

It is difficult to compare this to the experimental results of Vernon and Sage (1999) because they only examined radial migration. In addition, it is likely that the collagen matrix has a degree of anisotropy that introduces a bias (which is not accounted for in the mathematical model) for the cells to move predominantly in the equatorial plane ($z = 0$)[‖].

[§]Because of its dependence on the positions of the EC, which move stochastically, the collagen profile will not be exactly radially symmetrical, but the radial line plotted should be representative.

[‖]Phase-contrast microscopy shows that some of the collagen fibrils surrounding the EC aggregate in the RIMAC assay become radially aligned as a result of cellular traction. This is most likely a consequence of the supportive nylon mesh ring, which occupies the equatorial plane of the collagen matrix (Vernon, 2003). The radially aligned fibrils would offer less resistance to radial migration than to migration in the vertical direction (Dickinson *et al.*, 1994).

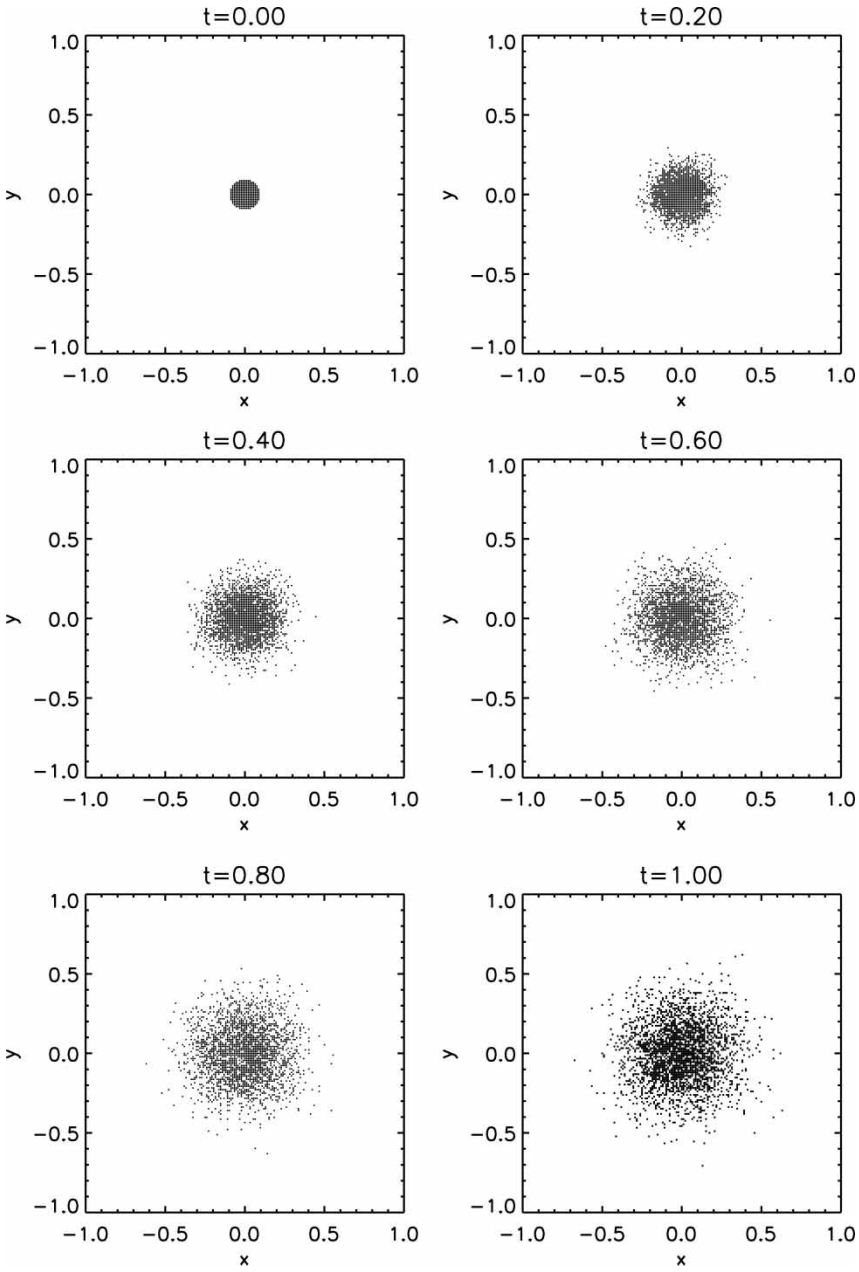

FIGURE 5 EC migration in the *xy*-plane in a simulation with the upper solution for VEGF (34) and $v_0 = 1$.

The two sets of simulations correspond to two extreme cases of the VEGF profile. The lower solution effectively corresponds to the case where VEGF uptake occurs throughout the matrix, whereas in reality uptake would only occur where EC are present. The upper solution corresponds to no uptake, and the VEGF profile is spatially uniform. To gain some insight into the possible intermediate behaviour, we also ran simulations with the full time-dependent upper solution (see appendix A). The results are shown in Fig. 12; the evolution of the VEGF profile may be seen in Fig. 13. Radial migration is less pronounced than with the steady state upper solution (Fig. 5), but more pronounced than with the lower solution (Fig. 11(a)). Conversely, vertical migration is greater than with the steady state upper solution (Fig. 6), but less than with the lower solution (Fig. 11(b)). This is unsurprising since, in the simulation using the time-dependent solution, there are both chemotactic and chemokinetic stimuli: chemotaxis is the dominant effect at the beginning of the simulation, when the VEGF concentration is low, but the concentration gradients are large; chemokinesis dominates towards the end of the simulation, when the gradients have been largely destroyed by diffusion, but the concentration has risen almost to v_0. In contrast, the lower solution is dominated primarily by chemotaxis, whilst the steady-state upper solution provides only a chemokinetic stimulus.

Recall from "The Model" section that we introduced a parameter, D_0, to which the continuum limit Eq. (10) is

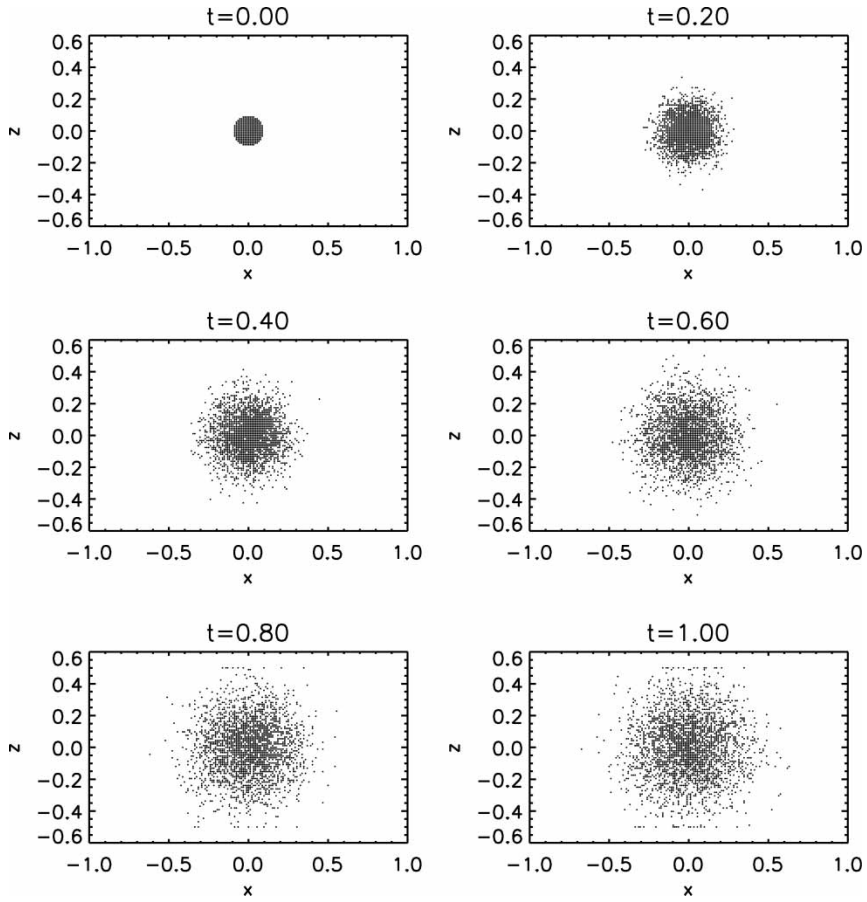

FIGURE 6 EC migration in the xz-plane in a simulation with the upper solution for VEGF (34) and $v_0 = 1$.

invariant, but which does affect the transition probabilities (25), (26), (29). In the simulations, we took D_0 to be the minimum value of $D(v)$, thus ensuring that $(D(v)/D_0) - 1 \geq 0$ and so the transition probabilities are always non-negative. This is the natural value to use, since the continuum limit Eq. (8) decomposes into a taxis term, with constant diffusion coefficient, D_0, and a random diffusive term, whose diffusion coefficient is the excess of $D(v)$ above D_0. Nevertheless, other choices, $D_0 < \min_{v \geq 0} D(v)$ are possible and it appears that reducing D_0 tends to reduce EC migration. This is a consequence of the finite grid size, h, and the dependence on D_0 vanishes in the limit $h \to 0$.

We now turn to the two-dimensional simulations of the system (22)–(30), (32), (35), (36). These include the full VEGF dynamics (23), with a point source of VEGF on the edge of the disc at $(x, y) = (-1, 0)$. The VEGF diffuses into the disc and establishes a chemotactic gradient, stimulating the EC to move towards $(-1,0)$. The effects of chemokinesis are still present, and so diffusive motion will be greater at higher VEGF concentrations. However, the introduction of a point source of VEGF should make the *directional* response of the EC, via chemotaxis, more apparent.

Figure 14 shows the results of a simulation with $v_0 = 1$[#]. The migration is clearly biased to the left as the EC move up the VEGF concentration gradient shown in Fig. 14(b); there is very little migration to the right.

As in the three-dimensional simulations, the collagen concentration is highest in the area corresponding to the initial EC aggregate. Thus haptotaxis will tend to hold the EC back (in contrast to chemotaxis, driving them towards the edge of this disc) and will therefore help to maintain the integrity of the central mass, which is still clearly visible at the end of the simulation. Note also that "cords" of raised collagen concentration appear to grow out of the central mass. These cords presumably mark the path of one or more EC, as they leave a trail of increased collagen in their wake. It is possible that, once established by leading cells, these cords act as preferred paths for following EC, because of the cells' affinity for collagen. This is a similar scenario to the slime-following myxobacteria model of Othmer and Stevens (1997).

Removing the VEGF source removes both the directional and the random diffusive stimuli and, unsurprisingly, there is very little migration (results not shown). Conversely, increasing the boundary concentration of VEGF ($v_0 = 2$, Fig. 15) increases the migration

[#]Note that, because we are effectively considering a two-dimensional cross-section through the full model, there are far fewer EC in the simulation.

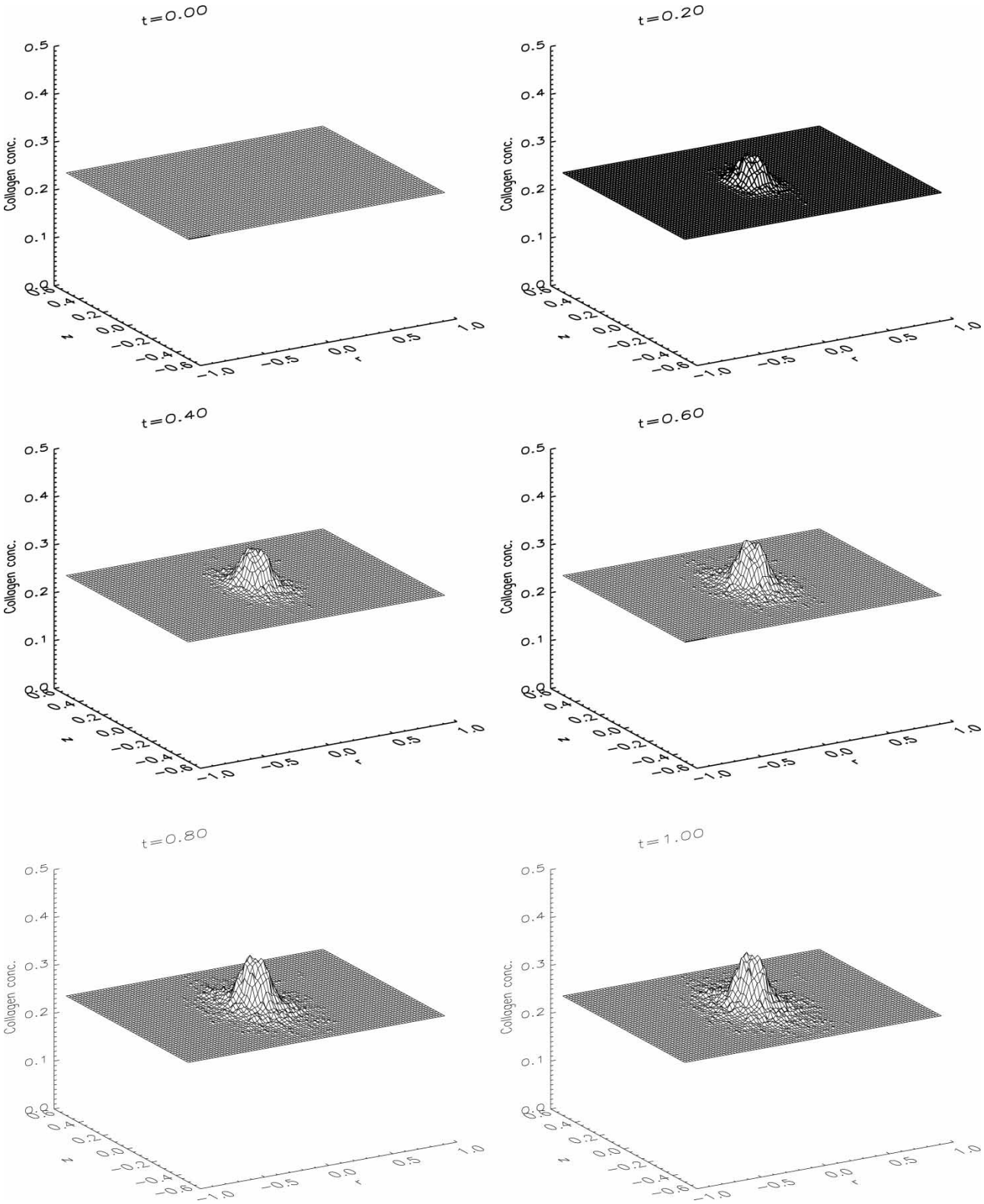

FIGURE 7 Evolution of the collagen profile in a simulation with the upper solution for VEGF (37) and $v_0 = 1$.

stimuli, resulting in greater invasion distances towards the point $(-1,0)$.

Removing the collagen (Fig. 16), however, removes haptotaxis and, in agreement with the hypothesis that haptotaxis helps to preserve the central mass, this results in its complete disintegration. This hypothesis is also borne out by the experimental results in Fig. 10(d), in which the collagen matrix is at a greatly reduced concentration. After just 2 days, the distances travelled are clearly larger than in Fig. 10(a), with some loss of

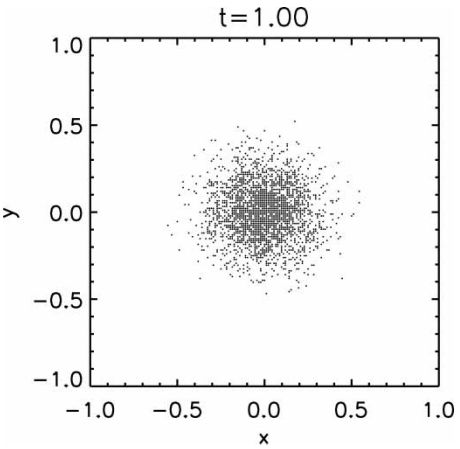

FIGURE 8 Positions of the EC after a simulation with the upper solution for VEGF (34) and $v_0 = 0.2$.

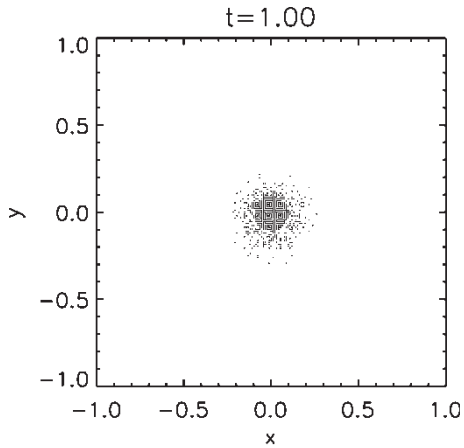

FIGURE 9 Positions of the EC after a simulation with the upper solution for VEGF (34) and $v_0 = 0$.

cell−cell adhesion. This may be partly due to the fact that it is more difficult for EC to penetrate denser collagen gels, and so reducing the matrix density facilitates invasion. Nevertheless, it was observed that the low collagen concentration used in Fig. 10(d) disrupted sprout branching and network formation.

Clearly, the role of ECM components, such as collagen, in angiogenesis is highly complex and far from fully understood. To assume that haptotaxis acts by stimulating EC to migrate up a collagen concentration gradient is a massive simplification. For example, there may be concentration-dependent effects of ECM components on EC random motility; this could be included in our model in a similar way to the chemokinetic effects of VEGF. Also, during angiogenesis *in vivo*, degradation of the ECM by EC-derived proteolytic enzymes is an important step, facilitating matrix invasion (Pepper, 2001). This has been included in several models, both continuous (Levine *et al.*, 2001) and discrete (Anderson and Chaplain, 1998).

The model has demonstrated good qualitative agreement with *in vitro* experimental results. We believe the reinforced random walk framework is ideal for studying cell migration and understanding the link between continuum (cell density) and discrete (individual cell-based) models. However, the correct functional form for the transition probability function, τ, which provides a link between the reinforced random walk master equation and its continuum limit, is not always clear and modelling

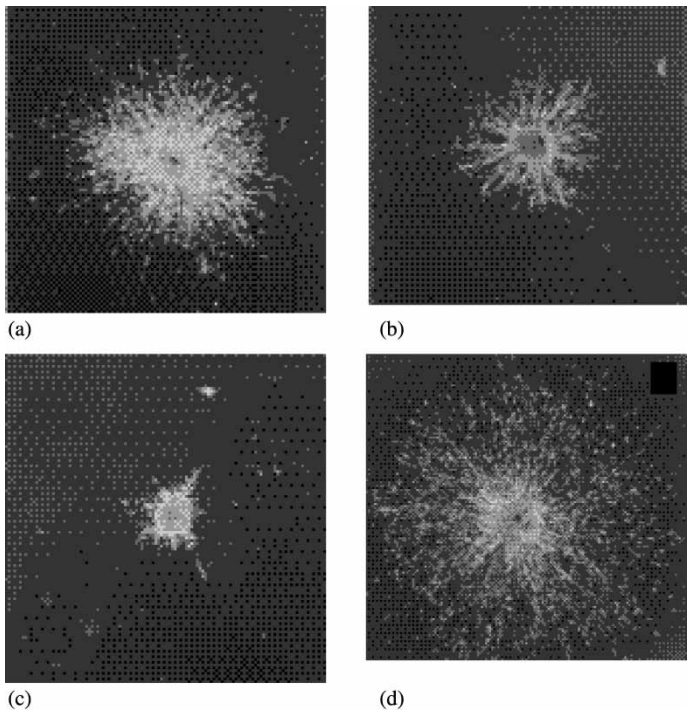

FIGURE 10 Experimental results of Vernon and Sage (1999): (a) VEGF concentration 5.0 ng/ml; collagen concentration 0.6 mg/ml; culture time 5 days. (b) Reduced VEGF concentration of 2.5 ng/ml; culture time 5 days. (c) No VEGF; culture time 5 days. (d) Very low collagen concentration; culture time 2 days.

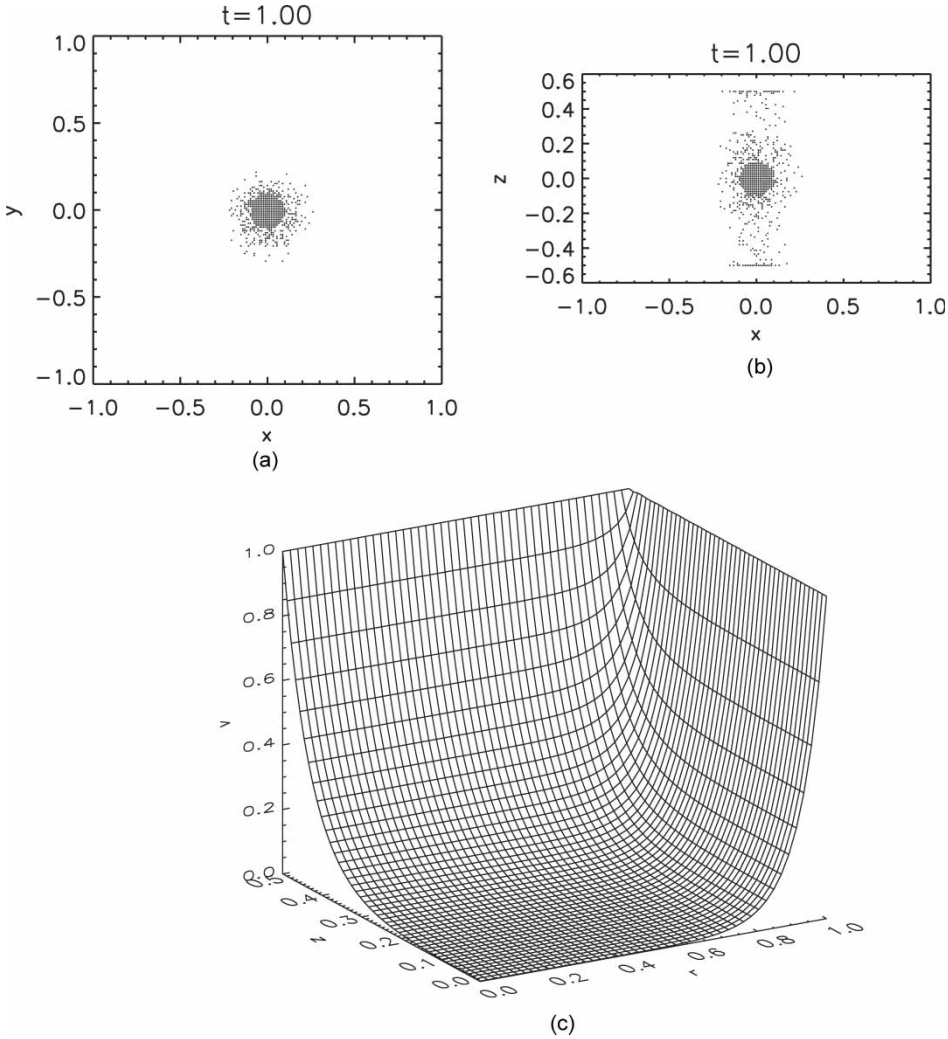

FIGURE 11 A simulation with the lower solution for VEGF (33) and $v_0 = 1$: (a) positions of the EC in the *xy*-plane. (b) positions of the EC in the *xz*-plane. (c) a graph of VEGF concentration against r and z.

chemotactic and chemokinetic effects in a biologically accurate way is an ongoing problem.

In this model, EC proliferation has been ignored but, during tumour angiogenesis, is a prerequisite for vascularisation (although initial sprouting can occur by EC migration alone) (Sholley *et al.*, 1984). In the experiment, no proliferation was observed at low VEGF concentration; significant proliferation was observed at

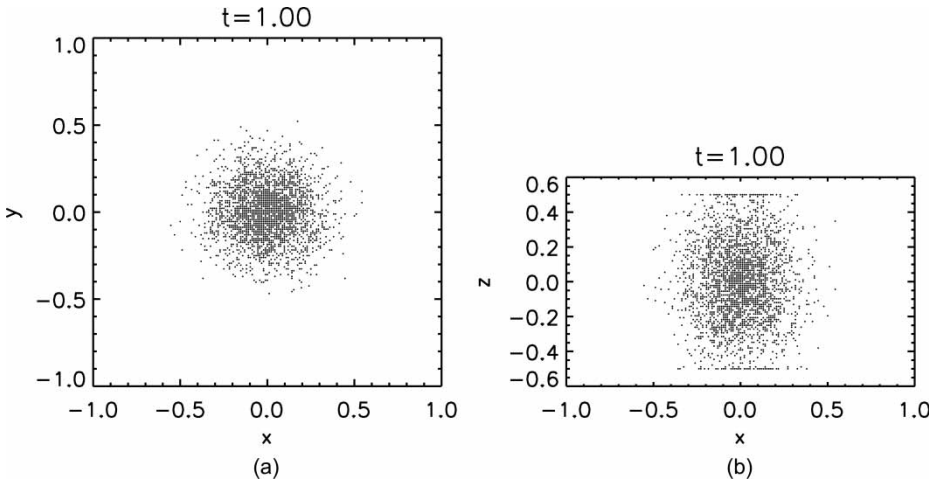

FIGURE 12 A simulation with the full time-dependent upper solution for VEGF and $v_0 = 1$: (a) positions of the EC in the *xy*-plane. (b) positions of the EC in the *xz*-plane.

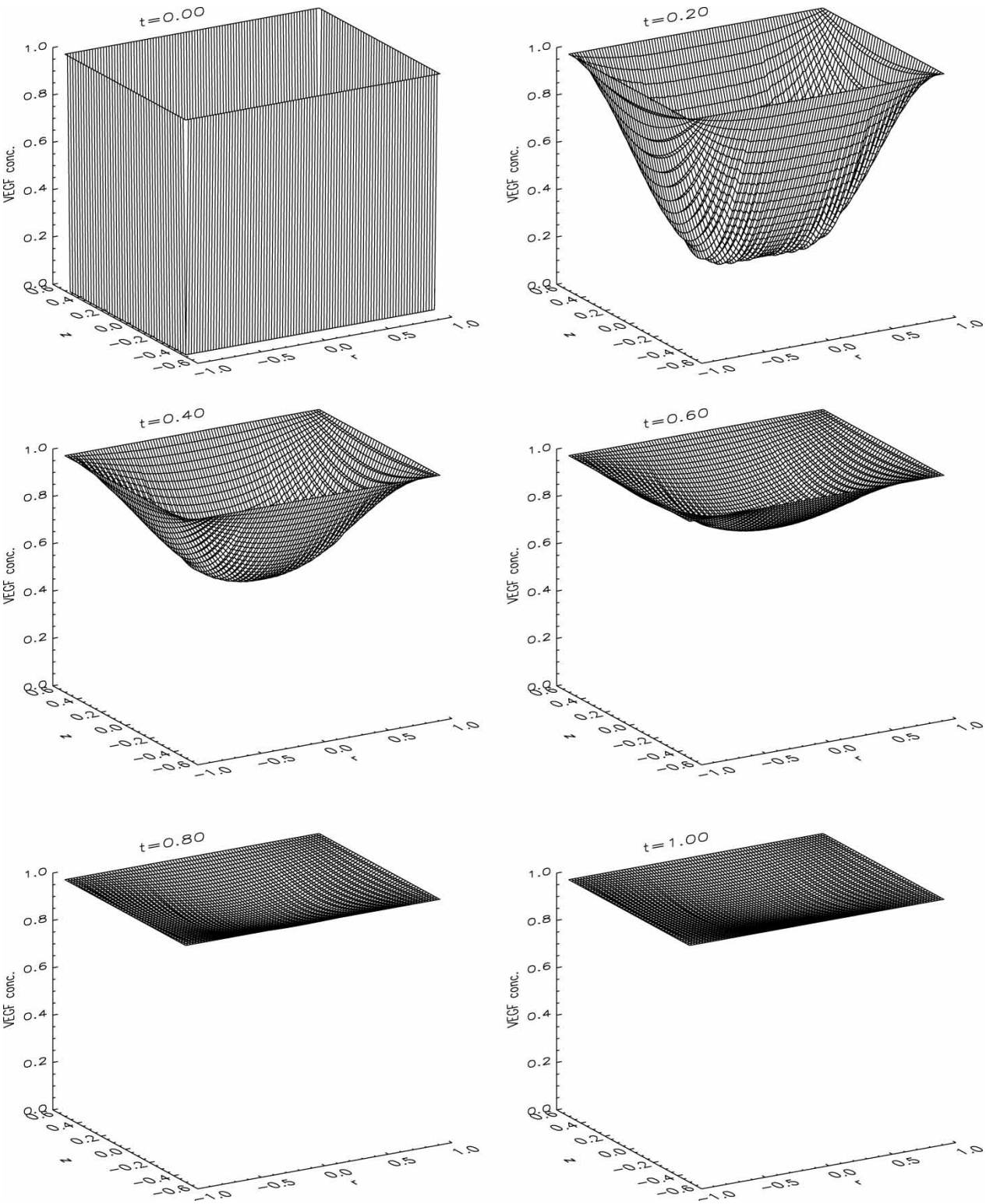

FIGURE 13 Evolution of the time-dependent upper solution for VEGF with $v_0 = 1$.

high VEGF concentration, although this was not crucial for matrix invasion. Including proliferation into this model would enlarge the invading EC population, but the mechanism one should use for proliferation in an individual cell-based model is not obvious. The simplest way would be to assume, for each cell, a constant probability of mitotic division per unit time (Sleeman and Wallis, 2002). A more realistic way would be to use an increasing function of VEGF concentration for the proliferation probability, since VEGF is known to be a mitogen for EC (Klagsbrun and D'Amore, 1996). However, it is unlikely that the complex cell signalling

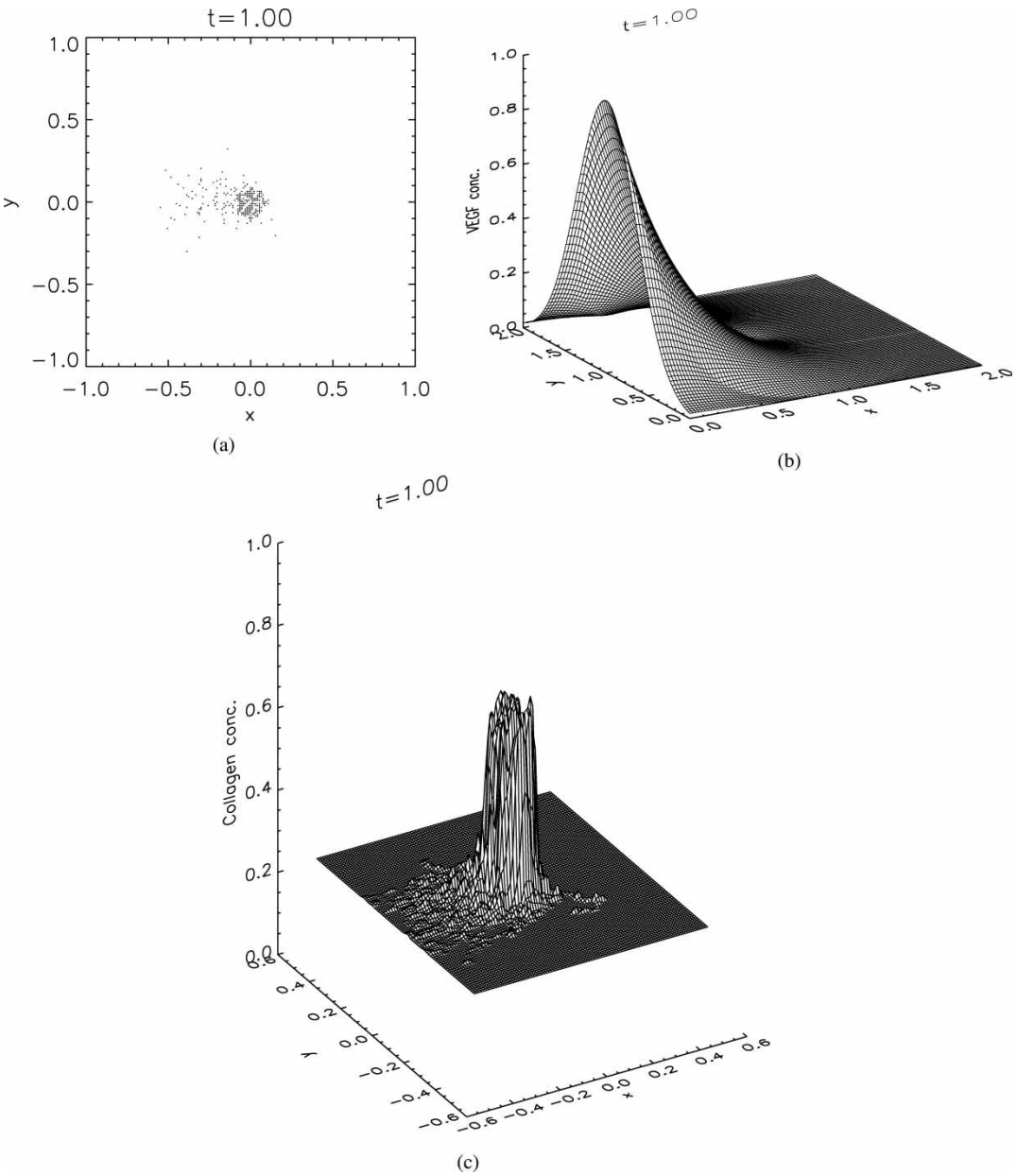

FIGURE 14 A simulation with a point source of VEGF at $(-1,0)$ and $v_0 = 1$: (a) positions of the EC. (b) VEGF concentration. (c) Collagen concentration.

processes involved can be fully captured by such simple mechanisms. More experimental data on the effects of angiogenic factors on EC proliferation rates is required before a comprehensive mathematical description can be incorporated into models of angiogenesis.

In the experiment carried out by Vernon and Sage (1999), the disc was immersed in medium, allowing growth factors to enter the collagen matrix from all sides. The symmetry of the setup thus made it difficult to distinguish between a chemokinetic response, in which EC movement would be purely random, and a chemotactic response, in which EC movement would be directed up a concentration gradient. It is likely that a combination of these two effects was at work, but the experiment can shed no light on their relative contributions to the overall migratory response. For this reason, we constructed a two-dimensional model of a hypothetical experiment, with a point source of VEGF on the edge of the disc. This enabled us to isolate and investigate the directional response of the EC to a diffusible angiogenic factor, which is a crucial component of tumour angiogenesis. It would be most interesting and enlightening to compare the predictions of this model to data from an *in vitro* experiment of this nature. This would allow the mathematical model to be refined, in close conjunction with empirical data, helping to determine accurate functional forms for the transition probability function,

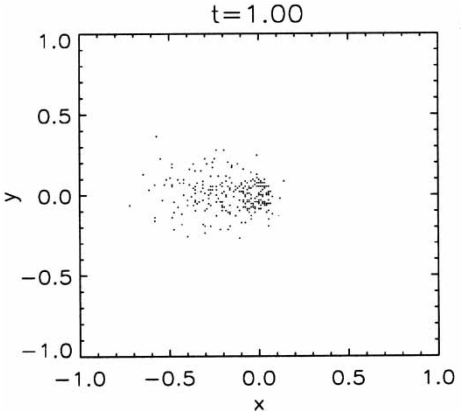

FIGURE 15 Positions of the EC after a simulation with a point source of VEGF at (− 1,0) and $v_0 = 2$.

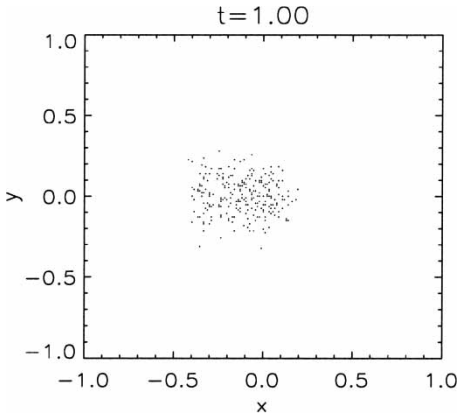

FIGURE 16 Positions of the EC after a simulation with a point source of VEGF at (− 1,0), $v_0 = 1$ and no collagen.

τ, and the EC diffusion coefficient. The relative importance of chemokinesis and chemotaxis in EC migration could thereby be elucidated.

Acknowledgements

The authors are indebted to Dr R.B. Vernon for clarifying experimental findings relating to the observed radial migration of cells. The authors would also like to thank Dr D. Read and Dr T. Liverpool for helpful discussions.

References

Alberts, B., Bray, D., Lewis, J., Raff, M., Roberts, K. and Watson, J.D. (1994) *The molecular biology of the cell*, 3rd Ed. (Garland, New York).

Anderson, A.R.A. and Chaplain, M.A.J. (1998) "Continuous and discrete mathematical models of tumour-induced angiogenesis", *Bull. Math. Biol.* **60**, 857–900.

Ausprunk, D.H. and Folkman, J. (1977) "Migration and proliferation of endothelial cells in preformed and newly formed blood vessels during tumour angiogenesis", *Microvasc. Res.* **14**, 53–65.

Balding, D. and McElwain, D.L.S. (1985) "Mathematical modelling of tumour-induced capillary growth", *J. Theor. Biol.* **114**, 53–73.

Bowersox, J.C. and Sorgente, N. (1982) "Chemotaxis of aortic endothelial cells in response to fibronectin", *Canc. Res.* **42**, 2547–2551.

Carmeliet, P. and Jain, R.K. (2000) "Angiogenesis in cancer and other diseases", *Nature* **407**, 249–257.

Carter, S.B. (1965) "Principles of cell motility: the direction of cell movement and cancer invasion", *Nature* **208**, 1183–1187.

Chaplain, M.A.J. and Stuart, A.M. (1993) "A model mechanism for the chemotactic response of endothelial cells to tumour angiogenesis factor", *IMA J. Math. Appl. Med. Biol.* **10**, 149–168.

Chaplain, M.A.J., Giles, S.M., Sleeman, B.D. and Jarvis, R.J. (1995) "A mathematical model for tumour angiogenesis", *J. Math. Biol.* **33**, 744–770.

Clark, R.A.F., DellaPelle, P., Manseau, E., Lanigan, J.M., Dvorak, H.F. and Colvin, R.B. (1982) "Blood vessel fibronectin increases in conjunction with endothelial cell proliferation and capillary ingrowth during wound healing", *J. Investig. Dermatol.* **79**, 269–276.

Davis, B. (1990) "Reinforced random walk", *Prob. Th. Rel. Fields* **84**, 203–229.

Denekamp, J. and Hobson, B. (1982) "Endothelial cell proliferation in experimental tumours", *Br. J. Cancer* **46**, 711–720.

Dickinson, R.B., Guido, S. and Tranquillo, R.T. (1994) "Biased cell migration of fibroblasts exhibiting contact guidance in oriented collagen gels", *Ann. Biomed. Eng.* **22**, 342–356.

Folkman, J. (1971) "Tumour angiogenesis: therapeutic implications", *New Engl. J. Med.* **285**, 1182–1186.

Folkman, J. (1974) "Tumour angiogenesis", *Adv. Canc. Res.* **19**, 331–358.

Folkman, J. and Klagsbrun, M. (1987) "Angiogenic factors", *Science* **235**, 442–447.

Giordano, F.J. and Johnson, R.S. (2001) "Angiogenesis: the role of the microenvironment in flipping the switch", *Curr. Opin. Genet. Dev.* **11**, 35–40.

Han, Z.C. and Liu, Y. (1999) "Angiogenesis: state of the art", *Int. J. Haematol.* **70**, 68–82.

Hanahan, D. and Folkman, J. (1996) "Patterns and emerging mechanisms of the angiogenic switch during tumourigenesis", *Cell* **86**, 353–364.

Hashizume, H., Baluk, P., Morikawa, S., McLean, J.W., Thurston, G., Roberge, S., Jain, R.K. and McDonald, D.M. (2000) "Openings between defective endothelial cells explain tumour vessel leakiness", *Am. J. Path.* **156**, 1363–1380.

Holmes, M.J. and Sleeman, B.D. (2000) "A mathematical model of tumour angiogenesis incorporating cellular traction and viscoelastic effects", *J. Theor. Biol.* **202**, 95–112.

Hunt, T.K., Knighton, D.R., Thakral, K.K., Goodson, W.H. and Andrews, W.S. (1984) "Studies on inflammation and wound healing: angiogenesis and collagen synthesis stimulated *in vivo* by resident and activated macrophages", *Surgery* **96**, 48–54.

Jackson, C.J., Jenkins, K. and Schrieber, L. (1992) "Possible mechanisms of type I collagen-induced vascular tube formation", In: Steiner, R., Weisz, P.B. and Langer, R., eds, *Angiogenesis: Key principles—Science–Technology–Medicine* (Birkhauser, Basel), pp 198–204.

Jones, D.S. and Sleeman, B.D. (2003) *Differential equations and mathematical biology* (CRC press, London).

Keller, E.F. and Segel, L.A. (1971) "Model for chemotaxis", *J. Theor. Biol.* **30**, 225–234.

Klagsbrun, M. and D'Amore, P.A. (1996) "Vascular endothelial growth factor and its receptors", *Cytokine Growth Fact. Rev.* **7**, 259–270.

Levine, H.A., Pamuk, S., Sleeman, B.D. and Nilsen-Hamilton, M. (2001) "A mathematical model of capillary formation and development in tumour angiogenesis: penetration into the stroma", *Bull. Math. Biol.* **63**, 801–863.

Liotta, L.A., Steeg, P.S. and Stetler-Stevenson, W.G. (1991) "Cancer metastasis and angiogenesis: an imbalance of positive and negative regulation", *Cell* **64**, 327–336.

Murray, J.D. (1993) *Mathematical biology*, 2nd Ed. (Springer, Berlin).

Muthukkaruppan, V.R., Kubai, L. and Auerbach, R. (1982) "Tumour-induced neovascularisation in the mouse eye", *J. Natl Cancer Inst.* **69**, 699–708.

Othmer, H.G. and Stevens, A. (1997) "Aggregation, blowup and collapse: the ABC's of taxis and reinforced random walks", *SIAM J. Appl. Math.* **57**, 1044–1081.

Paweletz, N. and Kneirim, M. (1989) "Tumour related angiogenesis", *Crit. Rev. Oncol. Haematol.* **9**, 197–242.

Pepper, M.S. (1997) "Manipulating angiogenesis", *Arterio. Thromb. Vasc. Biol.* **17**, 605–619.

Pepper, M.S. (2001) "Extracellular proteolysis and angiogenesis", *Thromb. Haemost.* **86**, 346–355.

Pepper, M.S., Belin, D., Montesano, R., Orci, L. and Vassalli, J.D. (1990) "Transforming growth factor-β1 modulates basic fibroblast growth factor-induced proteolytic and angiogenic properties of endothelial cells *in vitro*", *J. Cell Biol.* **111**, 743–755.
Plank, M.J. and Sleeman, B.D. (2003) "A reinforced random walk model of tumour angiogenesis and anti-angiogenic strategies", *IMA J. Math. Appl. Med. Biol.* **20**, to appear.
Reynolds, L.P., Killilea, S.D. and Redmer, D.A. (1992) "Angiogenesis in the female reproductive cycle", *FASEB J.* **6**, 886–892.
Risau, V. (1997) "Mechanisms of angiogenesis", *Nature* **386**, 671–674.
Schirrmacher, V. (1985) "Cancer metastasis: experimental approaches, theoretical concepts and impacts for treatment strategies", *Adv. Cancer Res.* **43**, 1–73.
Semenza, G.L. (2000) "HIF-1: using two hands to flip the angiogenic switch", *Cancer Metast. Rev.* **19**, 59–65.
Sherratt, J.A. and Murray, J.D. (1990) "Models of epidermal wound healing", *Proc. R. Soc. Lond. B.* **241**, 29–36.
Sholley, M.M., Ferguson, G.P., Seibel, H.R., Montour, J.L. and Wilson, J.D. (1984) "Mechanisms of neovascularisation", *Lab. Investig.* **51**, 624–634.
Shweiki, D., Itin, A., Soffer, D. and Keshet, E. (1992) "Vascular endothelial growth factor induced by hypoxia may mediate hypoxia-initiated angiogenesis", *Nature* **359**, 843–845.
Sleeman, B.D. and Wallis, I.P. (2002) "Tumour induced angiogenesis as a reinforced random walk: modelling capillary network formation without endothelial cell proliferation", *J. Math. Comp. Modelling* **36**, 339–358.
Stokes, C.L. and Lauffenburger, D.A. (1991) "Analysis of the roles of microvessel endothelial cell random motility and chemotaxis in angiogenesis", *J. Theor. Biol.* **152**, 377–403.
Vajkoczy, P., Farhadi, M., Gaumann, A., Heidenreich, R., Erber, R., Wunder, A., Tonn, J.C., Menger, M.D. and Breier, G. (2002) "Microtumour growth initiates angiogenic sprouting with simultaneous expression of VEGF, VEGF receptor-2 and angiopoietin-2", *J. Clin. Investig.* **109**, 777–785.
Vernon, R.B. (2003) Personal communication.
Vernon, R.B. and Sage, E.H. (1999) "A novel, quantitative model for study of endothelial cell migration and sprout formation within three-dimensional collagen matrices", *Microvasc. Res.* **57**, 118–133.
Yancopoulos, G.D., Davis, S., Gale, N.W., Rudge, J.S., Wiegand, S.J. and Holash, J. (2000) "Vascular-specific growth factors and blood vessel formation", *Nature* **407**, 242–249.

APPENDIX

Upper and Lower Solutions to the Reaction-diffusion Equation for VEGF

We use comparison principles to construct upper and lower functions for the solution to the PDE (23) for VEGF, subject to the initial and boundary conditions (31). The theorem we use may be stated as follows (Jones and Sleeman, 2003).

Suppose $w_1, w_2 : \Omega \times [0,T] \to \mathbb{R}$ (for $\Omega \subseteq \mathbb{R}^N$ and $0 < T \leq \infty$) are bounded continuous functions such that

$$\begin{aligned} \tfrac{\partial w_1}{\partial t} - \nabla^2 w_1 - f(w_1) &\leq \tfrac{\partial w_2}{\partial t} - \nabla^2 w_2 - f(w_2), && \text{on } \Omega\times[0,T], \\ w_1(x,0) &\leq w_2(x,0), && \text{on } \Omega, \\ w_1(x,t) &\leq w_2(x,t), && \text{on } \partial\Omega\times[0,T], \end{aligned}$$

where f is a continuously differentiable function.

Then either $w_1 \equiv w_2$ on $\Omega \times [0,T]$ or $w_1 < w_2$ on $\Omega \times [0,T]$.

By Eq. (23), we have

$$v_t - D_v \nabla^2 v + \alpha p v = 0, \quad \text{on } \Omega \times [0,1],$$

$$v(x,y,z,0) = \left\{ \begin{matrix} 0 & \text{inside } \Omega \\ v_0 & \text{on } \partial\Omega \end{matrix} \right\},$$

$$v(x,y,z,t) = v_0 \quad \text{on } \partial\Omega \times [0,1].$$

Now let $\hat{v}$ be such that

$$\hat{v}_t - D_v \nabla^2 \hat{v} + a\hat{v} = 0, \quad \text{on } \Omega \times [0,1], \tag{37}$$

$$\hat{v}(x,y,z,0) = \left\{ \begin{matrix} 0 & \text{inside } \Omega \\ v_0 & \text{on } \partial\Omega \end{matrix} \right\}, \tag{38}$$

$$\hat{v}(x,y,z,t) = v_0 \quad \text{on } \partial\Omega \times [0,1], \tag{39}$$

for some constant, $a \geq 0$.

By the above result, if $a \leq \alpha p$ ($a \geq \alpha p$) on $\Omega \times [0,1]$ then $\hat{v} \geq v$ ($\hat{v} \leq v$) on $\Omega \times [0,1]$. We now proceed to solve Eqs. (37)–(39). By radial symmetry and symmetry about $z = 0$, we need only consider

$$\hat{v}_t - D_v \left(\frac{1}{r}(r\hat{v}_r)_r + \hat{v}_{zz} \right) + a\hat{v} = 0,$$

$$\text{on } [0,1] \times [0,H] \times [0,1], \tag{40}$$

$$\hat{v}(r,z,0) = \left\{ \begin{matrix} 0 & 0 \leq r < 1, \;\; 0 \leq z < H \\ v_0 & \text{otherwise} \end{matrix} \right\}, \tag{41}$$

$$\hat{v}(1,z,t) = \hat{v}(r,H,t) = v_0, \tag{42}$$

$$\hat{v}_r(0,z,t) = \hat{v}_z(r,0,t) = 0. \tag{43}$$

Let $\hat{v}(r,z,t) = v_0(u(r,z,t) + g(r,z))$ where

$$D_v \left(\frac{1}{r}(rg_r)_r + g_{zz} \right) - ag = 0,$$

$$g(1,z) = g(r,H) = 1,$$

$$g_r(0,z) = g_z(r,0) = 0.$$

By separation of variables, we obtain

$$g(r,z) = \frac{\cosh\left(\sqrt{\frac{a}{D_v}} z \right)}{\cosh\left(\sqrt{\frac{a}{D_v}} H \right)} + \sum_{n=1}^{\infty} A_n I_0\left(\sqrt{\lambda_n} r \right)$$

$$\times \cos\left((2n-1) \frac{\pi z}{2H} \right), \tag{44}$$

where

$$A_n = \frac{16aH^2(-1)^{n+1}}{I_0(\sqrt{\lambda_n})\pi(2n-1)\left((2n-1)^2\pi^2 D_v + 4aH^2\right)},$$

$$\lambda_n = \frac{a}{D_v} + \frac{\pi^2(2n-1)^2}{4H^2},$$

and I_k is the modified Bessel function of the first kind and kth order.

Then by Eqs. (40)–(43),

$$u_t - D_v\left(\frac{1}{r}(ru_r)_r + u_{zz}\right) + au = 0,$$

$$u(1,z,t) = u(r,H,t) = 0,$$

$$u_r(0,z,t) = u_z(r,0,t) = 0.$$

We again use separation of variables to obtain

$$u(r,z,t) = \sum_{n=1}^{\infty}\sum_{m=1}^{\infty} B_{m,n}J_0(\omega_m r)\cos\left((2n-1)\frac{\pi z}{2H}\right) \times \exp\left(-D_v(\lambda_n + \omega_m^2)t\right), \quad (45)$$

where

$$B_{m,n} = \frac{8\pi(2n-1)D_v(-1)^n}{J_1(\omega_m)\omega_m\left((2n-1)^2\pi^2 D_v + 4aH^2\right)} - \frac{2A_n\omega_m I_0(\sqrt{\lambda_n})}{J_1(\omega_m)(\lambda_n + \omega_m^2)},$$

J_k is the Bessel function of the first kind and kth order, and $J_0(\omega_m) = 0$ $(m = 1,2,3,\ldots)$. This completes the solution of Eq. (40).

The dimensionless quantity, $p(x,y,z,t)$, is equal to 1 if an EC is present at (x,y,z) at time t, and is equal to 0 otherwise. Hence $a = 0$ and $a = \alpha$ are lower and upper bounds for αp on $\Omega \times [0,1]$ and substituting these values into Eqs. (44) and (45) gives an upper and a lower function respectively for the solution to Eq. (23).

Physically, the solution with $a = 0$ corresponds to the case where there is no VEGF uptake, and so the evolution of VEGF is governed only by diffusion. The solution with $a = \alpha$ corresponds to the case where EC are present throughout the matrix, resulting in a spatially uniform rate of VEGF uptake.

Clearly, the steady state of the solution, $\hat{v}_s(r,z) = v_0 g(r,z)$, is unique and is globally stable since

$$D_v(\lambda_n + \omega_m^2) > 0 \quad \forall m,n \geq 1.$$

The slowest decaying exponential in the time-dependent part of the solution (45) is $e^{-\sigma t}$ where

$$\sigma = a + D_v\left(\frac{\pi^2}{4H^2} + w_1^2\right).$$

For the lower function ($a = \alpha$), $\sigma = 49.644$ and so the solution evolves to the steady state (33) very rapidly. For the upper function ($a = 0$), $\sigma = 3.444$ and so evolution to the steady state (34) takes place more slowly, on a timescale that is comparable with the length of the experiment.

Discussion of Parameter Values

Diffusion coefficients: Sherratt and Murray (1990) used values in the range $2.48 \times 10^{-5}\,\text{mm}^2/\text{h}$–$1.26 \times 10^{-4}\,\text{mm}^2/\text{h}$ for the EC diffusion coefficient. Here we choose D_m, θ_1, θ_2 so that the diffusion coefficient is $D = 3.6 \times 10^{-5}\,\text{mm}^2/\text{h}$ for $v = 0$, and that $D \to 3.6 \times 10^{-4}\,\text{mm}^2/\text{h}$ as $v \to \infty$. Levine *et al.* (2001) took the diffusion coefficient for VEGF to be $D_v = 3.6 \times 10^{-3}\,\text{mm}^2/\text{h}$.

Time and length scales: The length of the experiment conducted by Vernon and Sage (1999) was $T = 5$ days $= 120$ h. The radius of the disc aperture (small assay) was $R = 1.4$ mm and its height was $2H = 1.4$ mm.

Grid size: EC are assumed to be incompressible cubes of side-length 0.015 mm, taken as an average value from Alberts *et al.* (1994). We therefore used a grid step size of 0.015 mm.

Size of EC aggregate: The aggregate used by Vernon and Sage (1999) consisted of between 1000 and 5000 cells, arranged in a sphere of radius r_i. Taking an average value of 3000 cells and assuming the cells are packed at maximum density, we have $\frac{4\pi r_i^3}{3} = 3000(0.015\,\text{mm})^3$ and so $r_i = 0.134$ mm.

VEGF and collagen concentrations: The standard level of VEGF applied by Vernon and Sage (1999) was $v_0 = 5 \times 10^{-3}\,\mu\text{g/ml}$. The initial collagen concentration was given as $c_0 = 600\,\mu\text{g/ml}$. We assume that the collagen concentration cannot increase by a factor of more than 4, and hence take the maximum collagen level as $C = 2400\,\mu\text{g/ml}$.

Reaction rates: The reaction rates, α and β, are difficult to specify accurately. We therefore take estimates based on reaction times as follows. If EC density is constant, the spatially uniform solution of the governing VEGF equation (17) can be written $v(t) = v_0 e^{-\alpha p t}$. Hence $\alpha = (\ln 2/p_0 T_h)$ where T_h is the half-life of VEGF at EC density, $p = p_0$. Half-lives for such reactions tend to be measured in hours (Levine *et al.*, 2001) and we assume this reaction is quite fast relative to the length of the experiment. We therefore estimate the half-life to be $T_h = 1.8$ h, which gives $\alpha = 8.66 \times 10^{-5}\,\text{mm}^2/\text{h}$.

Similarly, for p constant, the solution to the governing collagen Eq. (20) can be written $c(t) = (C/(C/c_0 - 1)e^{-\beta C p t} + 1)$. Clearly this tends to the maximum value, $C = 4c_0$, for large t, but let us make the reasonable assumption that, at EC density, $p = p_0$, the collagen concentration will triple over the course of the experiment, that is $c(T) = 3c_0$. This requires $3c_0 = (C/(C/c_0 - 1)e^{-\beta C p_0 T} + 1)$ and hence $\beta = (\ln 9/C p_0 T) = 1.72 \times 10^{-9}\,\text{mm}^2/\text{h ml}/\mu\text{g}$.

Chemotactic coefficient: Anderson and Chaplain (1998) used a chemotactic coefficient of 9.36×10^8 $\mathrm{mm}^2/\mathrm{h}/M$. Here the unit of chemical concentration, M, is a molar, or mole per litre. Levine *et al.* (2001) give the molecular weight of VEGF as 1.65×10^5 Da, so $1M$ is equivalent to 1.65×10^8 μg/ml. Converting the above figure of Anderson and Chaplain (1998) into these units gives a chemotactic coefficient of $\chi_0 = 5.67\ \mathrm{mm}^2/\mathrm{h\ ml}/\mu\mathrm{g}$.

Haptotactic coefficient: The value of the haptotactic coefficient, ρ_0, is unknown. We assume that VEGF is a stronger attractant than collagen, and therefore choose ρ_0 such that the haptotactic exponent, q_2, is one third of the chemotactic exponent, q_1, in Eq. (27).